COMITATO NAZIONALE PER L'ENERGIA NUCLEARE
Laboratori Nazionali di Frascati

LNF-72/71
2 Agosto 1972

B. Borgia, F. Ceradini, M. Conversi, M. Grilli, E. Iarocci, M. Nigro, L. Paoluzi, R. Santonico, P. Spillantini, L. Trasatti, V. Valente, R. Visentin and G. T. Zorn: MULTIHADRON PRODUCTION IN e^+e^- COLLISION AT HIGH ENERGY.

Servizio Documentazione
dei Laboratori Nazionali di Frascati del CNEN
Casella Postale 70 - Frascati (Roma)

Laboratori Nazionali di Frascati del CNEN
Servizio Documentazione

LNF-72/71
2 Agosto 1972

B. Borgia[o], F. Ceradini[o], M. Conversi[o], M. Grilli, E. Iarocci, M. Nigro[-], L. Paoluzi[o], R. Santonico[o], P. Spillantini, L. Trasatti[x], V. Valente, R. Visentin and G. T. Zorn[x]: MULTIHADRON PRODUCTION IN e^+e^- COLLISION AT HIGH ENERGY.

1. - INTRODUCTION -

The development of electron-positron storage rings of total energy in the GeV region has made possible the direct investigation of processes involving virtual photons in the deep time-like region. The reactions resulting from the e^+e^- collisions proceed in the one-photon approximation through a state of well defined quantum numbers ($J^{PC}=1^{--}$) and this selects the possible final states[1]. Elegant and accurate experimental studies of well-established vector mesons with these quantum numbers (ϱ, ω, ϕ) have become possible and have been carried out in recent years, at Novosibirsk with VEPP 2[2] and at Orsay with ACO[3].

Investigations of this type at higher energy are of the greatest interest, not only because they represent a search for other possible resonances with higher masses, but also because of possible linkages with deep electron-proton inelastic scattering[4], when the asymptotic region is reached[+].

The successful operation of "Adone"[5], the Frascati 2x1.5 GeV e^+e^- storage ring, has made it possible to accomplish a first step along these lines. As will be seen later on in this article, this has been accomplished through the study of the multihadronic reactions

(1) $$e^+e^- \rightarrow m(h^+h^-)+nh^o$$

(o) - Università di Roma, and INFN, Sezione di Roma.
(-) - Università di Padova, and INFN, Sezione di Padova.
(x) - Dept. of Physics and Astronomy, Univ. of Maryland. - Work partly supported by the U.S.A.E.C.
(+) - This point will be further discussed in Sec. 11.

where $m \geq 1$, $n \geq 0$, $m + n \geq 2$ and h^+, h^-, h^o are assumed to be pions for reasons explained later. The investigation of the two-body hadronic process $e^+e^- \rightarrow h^+h^-$, has been performed by our group ($\mu\pi$) and BCF group at Adone[6]. The results on this reaction will be the subject of separate papers[7].

Multi-hadron production was observed at Adone, and independently at Novosibirsk, early in 1970. It was first reported at the Kiev International Conference[8]. These preliminary results have been substantially confirmed by subsequent experimentation leading to better estimates[9],[10],[6a],[11],[12] of the cross sections for the reactions (1).

An interesting feature of the results obtained at Adone and reported in detail in the present article, is the relatively large value of the total cross section for multi-hadron production. Over the center-of-mass energy interval explored, $1.2 \leq 2E \leq 2.4$ GeV, (where $2E = E_+ + E_-$ is the total energy of the colliding beams) this cross section appears to be comparable with, or at highest energies, possibly greater than the cross section, $\sigma_{\mu\mu}$, for e^+e^- annihilation into muon pairs. We recall that $\sigma_{\mu\mu} = 21/E^2$ nb (1 nb = 10^{-33} cm^2) if E is expressed in GeV.

Unfortunately, due mostly to the rather large errors associated with the present data, it is difficult to decern possible structures in the energy dependence of σ_{tot}. Nevertheless, for the specific annihilation channel which has only four charged pions in the final state, our group has observed a broad peak[13], in the energy dependence of the production cross section. The observed behaviour of the cross section is consistent with the hypothesis of a ρ' meson[14] of mass $m_{\rho'} \approx 1.6$ GeV and width $\Gamma_{\rho'} = \sim 350$ MeV. Such an hypothesis will be further discussed later in this article, also in the light of other recent experimental results obtained at SLAC(x).

After a description of the experimental apparatus in Sec. 2, the results of measurements performed with electrons of known energies in order to obtain a calibration of the apparatus itself are given in Sec. 3. The subsequent Sec. 4 describes the scanning and the event selection. Background problems are discussed in Sec. 5, and Sec. 6 is devoted to a phenomenological classification of the events. In Sec. 7 the nature of the secondary particles and reactions is analyzed and in Sec. 8 a Monte carlo simulation of the experiment is described. In view of the possible existence of a ρ' meson, a detailed analysis of the specific reaction $e^+e^- \rightarrow \pi^+\pi^-\pi^+\pi^-$ is made in Sec. 9. Results are presented in Sec. 10

(x) - We wish to thank Professor John J. Sakurai for communicating to one of us (M.C.) the preliminary results of the SLAC experiment based on use of back scattered laser photon beams (see Sec. 11).

and discussed in Sec. 11 which ends with a list of conclusions.

2. - EXPERIMENTAL APPARATUS -

The experiment was carried out at one of the four experimental straight-sections of Adone. Measurements were taken for values of the beam energy, E, in the range .6-1.2 GeV. The beams collided head-on in the center of the experimental straight section. The collision region was assumed to have a gaussian distribution in all directions. Its transversal dimensions were of order of 1 mm, while its longitudinal standard deviation was found by us[15] to be $\delta = 20 \pm 1.5$ cm at E = 1 GeV, in agreement with the measurements by the machine group[16]. The quantity δ increased with energy[17] approximately as $E^{3/2}$. The collision time of the e^+ and e^- bunches was $\sim$ 2 ns and the time between two consecutive collisions was $\sim$ 117 ns. In the beam energy interval covered during this experiment, the machine luminosity, L, increased steeply with beam energy[x]. At E = 1 GeV/beam $L \sim 10^{33}$ cm^{-2} Hr^{-1} at injection. The meanlife of the beams, on the contrary, decreased with increasing E and it was typically about 10 hours at E = 1 GeV.

Drawings of two projected views of the main apparatus are given in Fig. 2.1. Additional equipment, not shown in Fig. 2.1, was also installed at the same straight-section: (a) a monitoring system[18][8a], which was used to measure continuously the machine luminosity by means of the Bhabha scattering at small angles; a process which is supposed to be correctly described by quantum electrodynamics since it involves small momentum transfers; (b) a device[19] to investigate experimentally by a tagging technique, the reactions

$$e^+e^- \rightarrow e^+e^- + (\text{hadrons, leptons}) \qquad (2)$$

which have received recently considerable interest[20÷22].

The main apparatus was made up of two telescopes located on opposite sides of the straight section of the machine. From a point at the center of the straight section, both telescopes covered nearly 1/4 of the total solid angle. Each telescope was composed of scintillation counters ($E_i(I_i)$, i = 0, ..., 5), Cerenkov counters (C_E, C_I), optical spark chambers (C_1, C_2, C_3, C_4) and lead and iron absorbers. Additional counters, A and B, were placed above and below the vacuum chamber in order to increase the solid angle for the detection of multiparticle final states. They were not required, however, in the formation of the master trigger (eq. (3))

(x) - As shown in ref. 16) the average luminosity changed from 6.10^{31} to 6.10^{32} cm^{-2} h^{-1} when E increased from 0.7 to 1.2 GeV/beam.

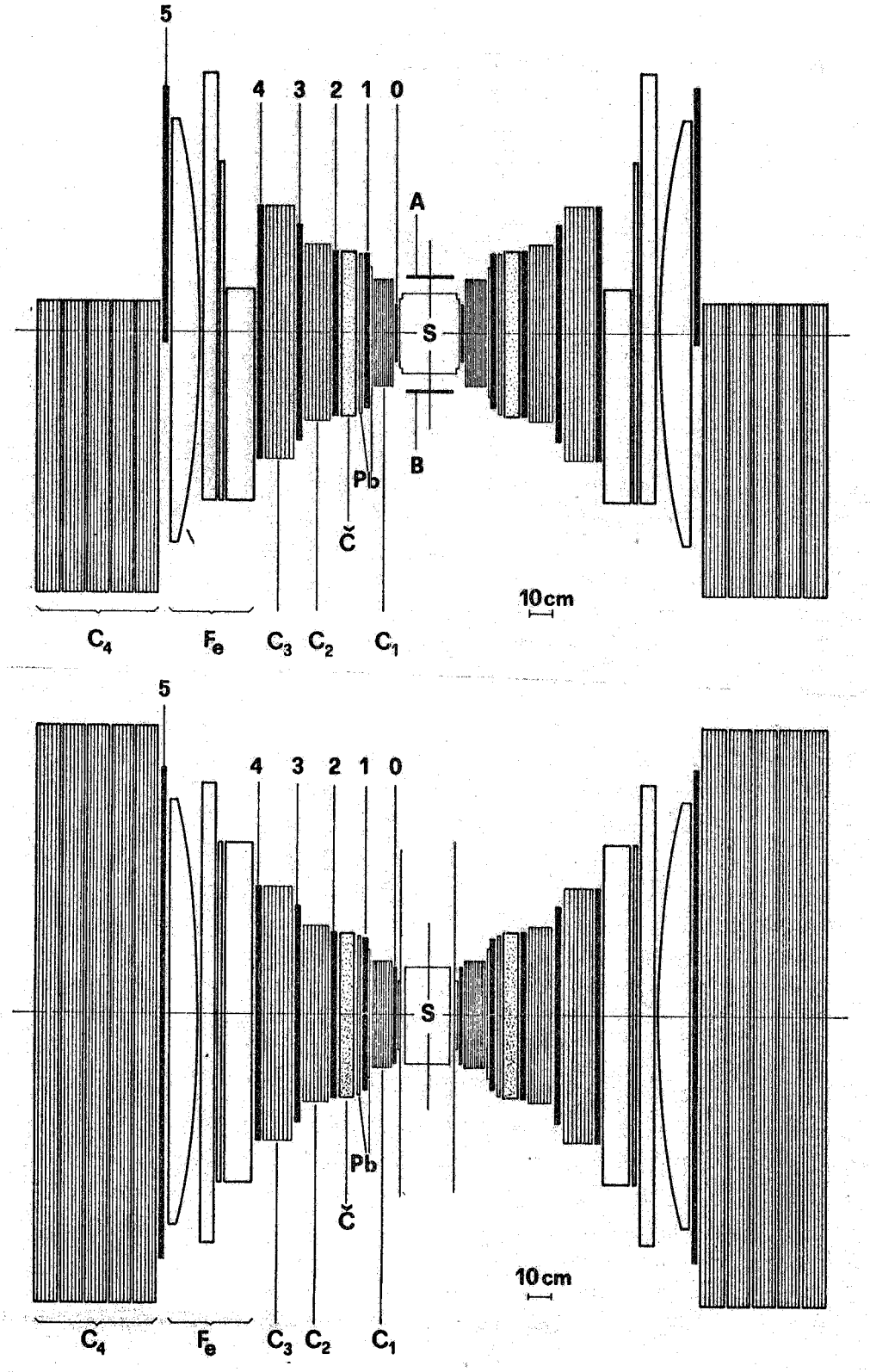

FIG. 2.1 - Schematic views of the apparatus. C_1 are thin foil spark chambers used for space reconstruction of the events. C_2, C_3 and C_4 are thick plate spark chambers used to observe the development of electromagnetic showers and/or the interactions and stop of charged particles. Č are water Cerenkov. Counters numbered from 0 to 5 are scintillator counters. A and B are scintillation placed above and below the vacuum chamber to increase the solid angle for multibody events. S, the "source", is the crossing region of the bunches.

for the spark chambers and the camera film advance.

The optical system is briefly described in Appendix A. The two orthogonal views of the chambers, shown in Fig. 2.1, togheter with all relevant information, were recorded on a single 70 mm x 100 mm frame.

Fig. 2.2 gives the sequence of thicknesses, in g/cm^2, of the various elements present in the telescopes (see, also, Table A1 and Table A2, in Appendix A).

The first spark chambers, C_1, are thin foil chambers used for the spatial reconstruction of tracks. C_2 and C_3 are thick-plate spark chambers which were essential for the identification of particles by observation of their behaviour in traversing them (see Sec. 3). The end spark chambers, C_4, are also thick plate chambers covering $\sim$ 50% of the solid angle of the telescopes(x). The thickness of the iron absorber

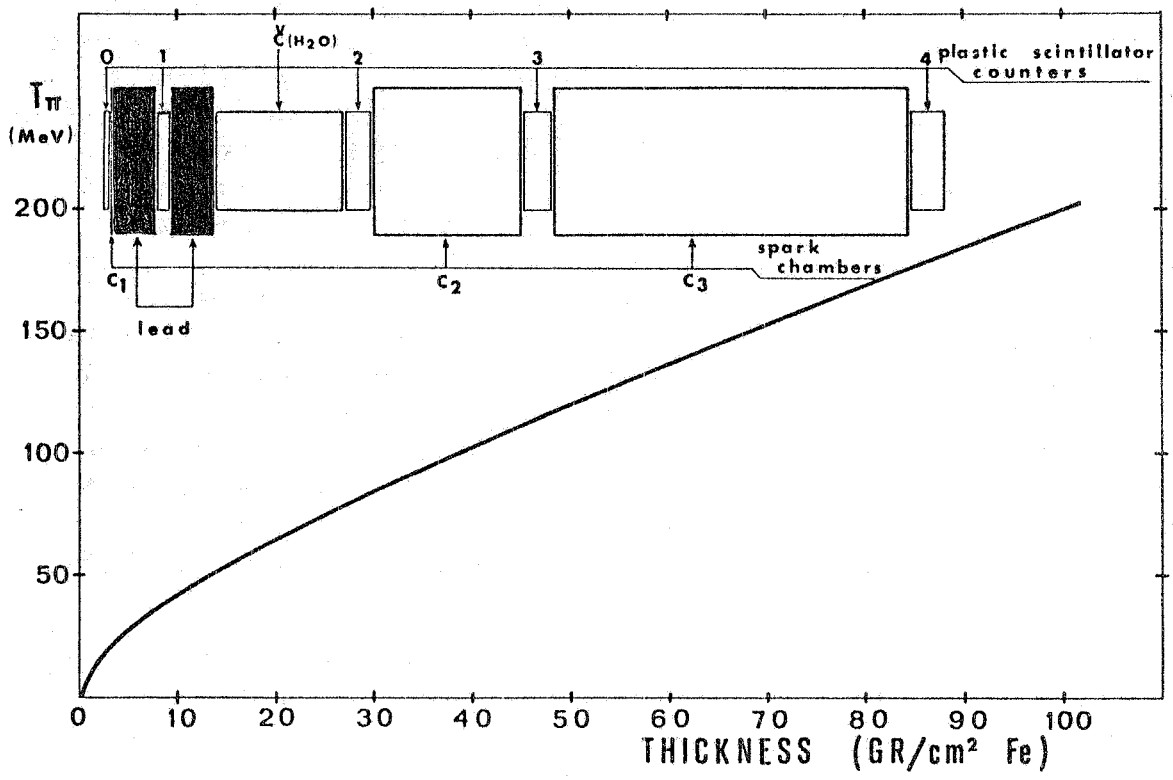

FIG. 2.2 - Minimum kinetic energy T_π, of a charged pion for a given penetration in a telescope. Counter 5, not shown, is placed after 380 g/cm^2, i.e. corresponds to $T_\pi \sim$ 605 MeV. Thickness of various elements is given in equivalent thickness of Iron.

(x) - The weight of each telescope was in excess of 20 tons and for obviously practical reasons it was not feasible (nor necessary) to extend the thick plate end chambers, C_4, above the horizontal median plane.

placed before chamber C_4 in each telescope, was adjusted as the beam energy changed, so that muons from process $e^+e^- \rightarrow \mu^+\mu^-$ stopped in these chambers[23]. On the contrary, pions from $e^+e^- \rightarrow \pi^+\pi^-$, or from multihadronic events, with high probability undergo nuclear interactions in the preceeding absorber and essentially do not reach C_4.

The logic involved in triggering the optical spark chambers was rather complex, essentially for two reasons. First we wanted to detect multibody events, simultaneously with the collinear events associated with two-body final states, i.e. e^+e^-, $\mu^+\mu^-$, $\pi^+\pi^-$, K^+K^-. Secondly, the rate of cosmic rays traversing the two telescopes was slightly in excess of one per sec, far greater than that for events produced by the collisions of e^+ and e^- bunches. A strong rejection against cosmic rays was therefore needed, not only to avoid a possible source of background for the process $e^+e^- \rightarrow \mu^+\mu^-$[23], but also in order to keep the triggering rate of the film advance at a reasonable value of a few per minute(+).

The need to select the various types of e^+e^- events with high efficiency, combined with the necessity of an efficient rejection of cosmic rays, forced us to use two different triggers. The first was designed for the detection of the annihilation events $e^+e^- \rightarrow \mu^+\mu^-$, and the second for the detection of all other events. The rejection of cosmic rays was based on three requirements, of which only the first was common to both triggers. These requirements were: a) correct timing, relative to the instant of collision of the e^+, e^- bunches, achieved by exploiting the phase of a signal (RF) from the machine radiofrequency; b) correct time-of-flights between the two counters 3 and between the two counters 4 of the two telescopes, two counter pair being traversed simultaneously only by particles from two-body events[24]; c) absence of a signal from either of two counters 5. In order to avoid any appreciable loss of e^+e^- events both conditions a) and b) were imposed with time windows increased by a substantial factor. More stringent time criteria subsequently were applied, however, during the analysis of the events, as all time-of-flights were measured and recorded in digital form on each photograph.

The trigger logic used to detect the various types of events is explained in Appendix A. In order to suppress the rate of picture taking, we were forced to use a high-order coincidence and some amount of absorber between counters. This amount was chosen as a compromise between the need to decrease the machine background, and the desire to minimize the loss of multi-hadron events. The following 8-fold master

---

(+) - At the occurrence of a trigger coincidence the electronics was "paralized" for $\sim$ 3 sec to allow full recovery of the H.T. power supplies (App. A). A triggering rate of more than a few per minute would therefore result in an untolerable loss of events.

coincidence, M_{mh}, was used to select multi-hadron events:(x)

$$M_{mh} = E_o I_o E_1 I_1 E_2 I_2 (E_3+I_3)\cdot(E_4+I_4)\cdot\overline{(E_5+I_5)}\cdot RF \qquad (3)$$

where E_i and I_i (i= 0, 1, 2 ... 5) represent respectively the signals from the scintillation counters in the external and internal telescopes, as shown in Fig. 2, 1, and RF is the radiofrequency phase signal from the machine as previously mentioned.

As one can see from Eq. (3), the minimum penetration required for charged particles to produce the coincidence M_{mh}, is up to counter 2 of one telescope and up to counter 4 of the opposite telescopes. As seen in Fig. 2.2 the corresponding minimum kinetic energies for pions are 90 MeV and 185 MeV, respectively.

All spark chambers were triggered and the film was advanced on the occurrence not only of the trigger M_{mh}, but also of the other trigger, $M_{\mu\mu}$. The latter trigger was used in selecting muon pairs and is described in Appendix A.

All counters were so operated that minimum-ionizing particles traversing any part of the scintillator were recorded with an efficiency greater than 99% by the logic circuitry. The time resolution for the master coincidences was $\sim$ 10 ns (half-width at half maximum), which is small when compared with the time between two consecutive collisions of e^+e^- bunches, i.e. 117 ns.

In addition to the side and top views of all spark chambers, a data box also was photographed. The following information was presented in digital form in the data box:

a) date and time;
b) frame number;
c) pattern of coincident pulses from counters $E_o, I_o; E_3, I_3; E_4, I_4; E_5, I_5$; $\check{C}_E, \check{C}_I$; A and B.
d) time between instant of a bunch-bunch collision and a pulse of either of counters 1; T_{1RF}.
e) sum of pulse heights in counters I_2 and I_3, (called H_I), and E_2 and E_3, (called H_E);
f) delay times between the two counters E_3 and I_3, called T_{33}, and between the two counters E_4 and I_4, called T_{44};
g) counting rate of luminosity monitor, integrated from the beginning of the run until the time of the photograph.

For further details on the apparatus see Appendix A.

(x) - This type of trigger was used during most of the measurements when Adone was operated in the energy interval $1.5 \lesssim 2E \lesssim 2.0$ GeV. Other trigger master coincidences which were used outside this energy interval are given in Appendix A.

3. - CHECKS AND CALIBRATION OF THE APPARATUS -

Due to the complexity of the apparatus previously described, it was essential to test continuously its performance using information registred on scalers, nixie-lamps and multi-channel analyser, and also by making stability checks. The latter were done daily with cosmic ray runs, while Adone was not operating. Some of the typical distributions are given below.

In Fig. 3.1 examples of distributions of the time-of-flight T_{1RF}, for cosmic rays and wide angle Bhabha scattering (WAS events) are shown. Pulse-height distributions for counters 2 and 3 were also recorded during both machine and cosmic-ray runs. Examples of such distributions are given in Fig. 3.2. Similarly the time-of flight distributions T_{33} and T_{44} were also recorded during both types of runs. These distributions were used for the interpretation of the collinear events and have been discussed in previous pubblications[15][23].

In addition to the on-line checks and calibrations, special calibration runs, already partially described elsewhere[9a], were made with electrons from the Frascati 1 GeV Electron-synchrotron. The purpose of these runs was to determine the response of spark chamber-counter telescopes to electrons of various energies. For these tests spare spark chambers and counters identical to those used in Adone were used to set-up one of the two actual telescopes up to chamber C_3. Calibration measurements were performed on it for electron energies, E_e, between 50 MeV and 500 MeV. The response of the telescopes to electrons of energies $E_e \gtrsim 600$ MeV was obtained from WAS events recorded in the main runs carried out at Adone, so that there was no need for special calibration measurements at these higher energies.

The probabilities, P_2 and P_3, that an electron gave a signal, respectively, in counters 2 and in both counters 2 and 3 of the apparatus, were determined for each energy value. These probabilities are reported in Fig. 3.3 as a function of the energy E_e. A first conclusion resulting from these measurements is that electrons of energy below 200÷250 MeV have but a small probability of triggering the apparatus through the master coincidence M_{mh}, defined in Sec. 2.

In order to observe in a statistically significant way the behaviour of the electrons in the shower chambers C_2 and C_3, a total of about 1000 pictures were taken. The analysis of these photographs was rather detailed since criteria derived from it allowed us to distinguish electrons from hadrons in the observed multi-particle events.

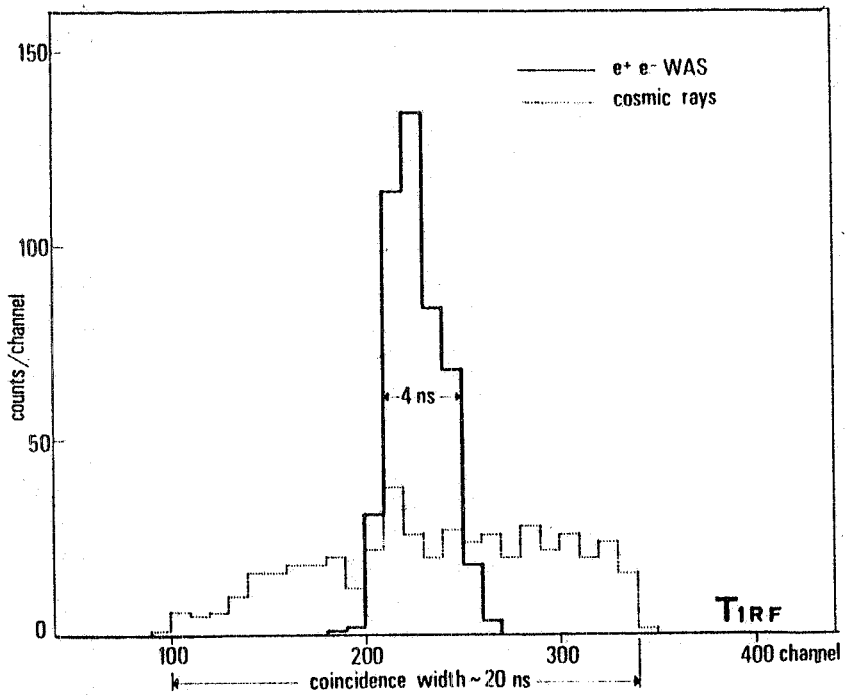

FIG. 3.1. - Distribution of time of flights, T_{1RF}, between either one of counters 1 and the RF phase signal, for cosmic rays and wide angle Bhabha scattering events (WAS).

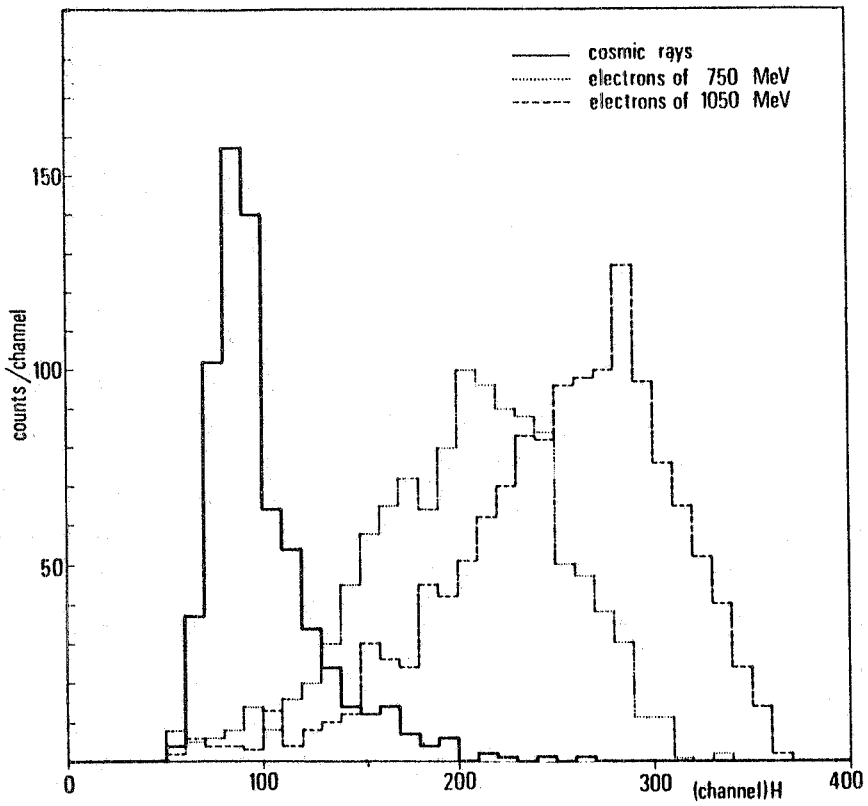

FIG. 3.2. - Distribution of pulse heights, $H_E(I)$, for cosmic rays and electrons of given energies.

In the analysis of spark chamber pictures the following definitions were introduced: (a) a group of n non aligned sparks appearing in more than two gaps and within an angle of 15° from the primary electron, is called a shower; (b) n sparks aligned along the primary-electron direction is called a single track. It should noted, however, that if $n < 3$ it was not found to be possible to distinguish between a shower and a single track.

Also in this analysis events were divided into two categories: i) events with coincident pulse in counter 2 but none in counter 3, and ii) events with coincident pulses in both counters 2 and 3. The probabilities for the occurrence of i) and ii) were indicated (Fig. 3.3) previously as P_2 and P_3, respectively.

Category i). - The fraction of events of this type that have less than 3 sparks ($n < 3$) appearing in the spark chamber C_2 is given in Fig. 3.4 as a function of electron energy, E_e. About 5% of electrons in this category at all energies produce single tracks with $n \geqslant 3$ in C_2. The remaining events give rise to showers with $n \geqslant 3$, as defined above.

Category ii). - This category presents fewer difficulties in event classification than category i) as both spark chambers C_2 and C_3 are considered and, consequently, on the average there are more sparks to be utilized in the analysis. The average number of sparks in showers produced by electrons in chambers C_2 and C_3 as a function of electron energy is given in Fig. 3.5. In the same figure the fluctuation in this number about the average also are indicated by max and min. curves. On the basis of these results, the minimum number of sparks to be used in identifying showers was set at four, i.e. $n \geqslant 4$.

The results of an analysis of events of category ii) are presented in Fig. 3.6. Curve 1 gives the probability that an electron produces a shower ($n \geqslant 4$); curve 2 a single track, and curve 3 an ambiguous result. Curve 4 is the sum of curves 1 , 2 and 3 and is the probability P_3 (of Fig. 3.3) that an electron produces signals in counters 2 and 3. Thus, for those events in which counters 2 and 3 are required in the trigger, the probabilities for incident electron are given in this figure for the different spark configurations at each energy E_e. By using a more restrictive definition of a single track, requiring $n \geqslant 6$, a greater certainty in particle identification is possible. This can be seen in Fig. 3.7, where the probability that an electron gives a pulse in counters 2 and 3 and produces a single track with $n \geqslant 6$ is presented.

The results discussed in this section furnish the basis for particle identification throughout this paper.

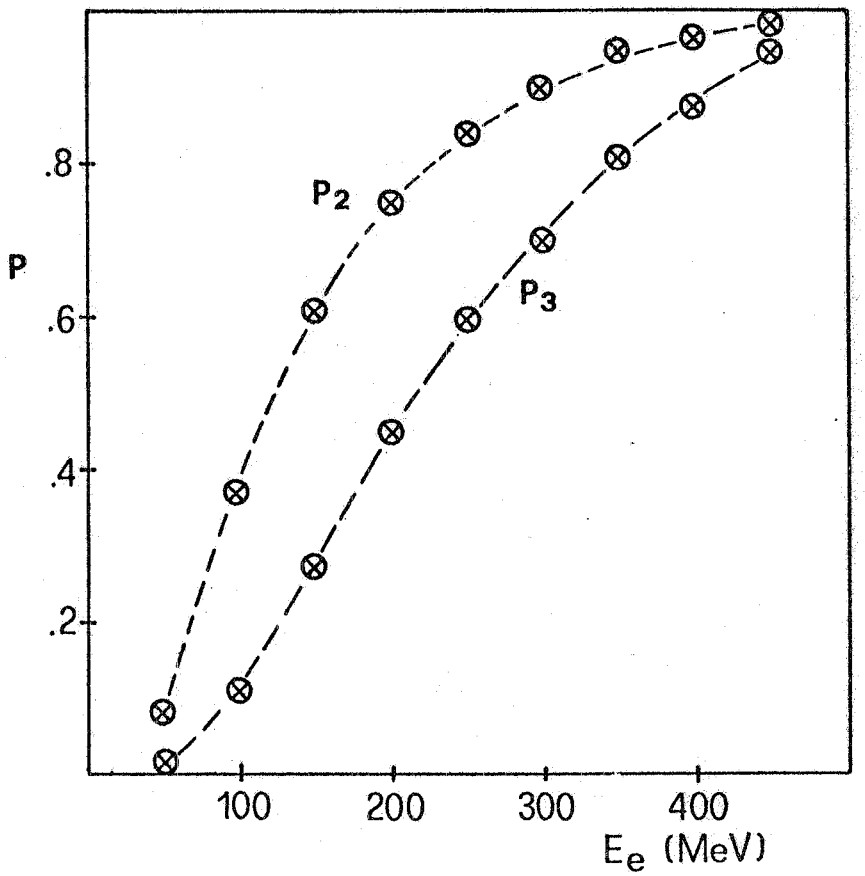

FIG. 3.3 - The probabilities for an electron to produce a pulse in counter 2, P_2, and in both counters 2 and 3, P_3, as a function of its energy, E_e.

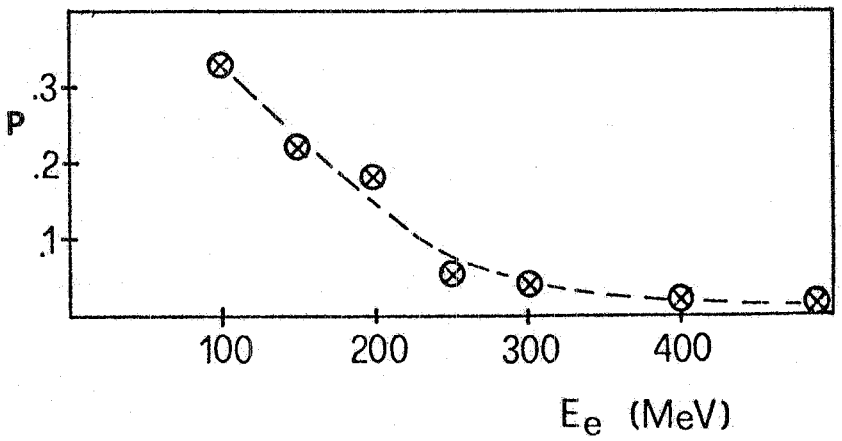

FIG. 3.4 - Probability for an electron giving a pulse in counter 2 and not in counter 3 to produce less than 3 sparks in spark chamber C_2.

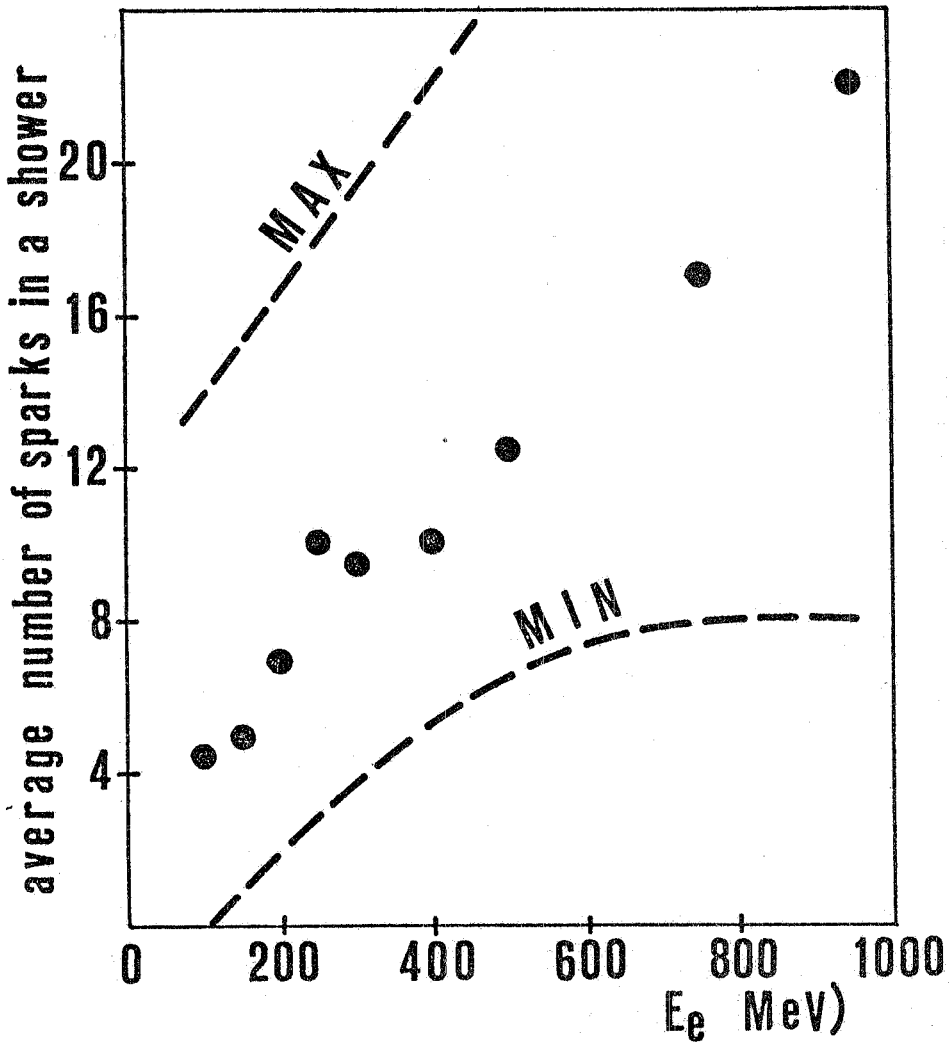

FIG. 3.5 - Average number of sparks in showers appearing in chambers C_2 and C_3 per electron of energy E_e which have produced a pulse in counters 2 and 3. Maximum and minimum limits are also given.

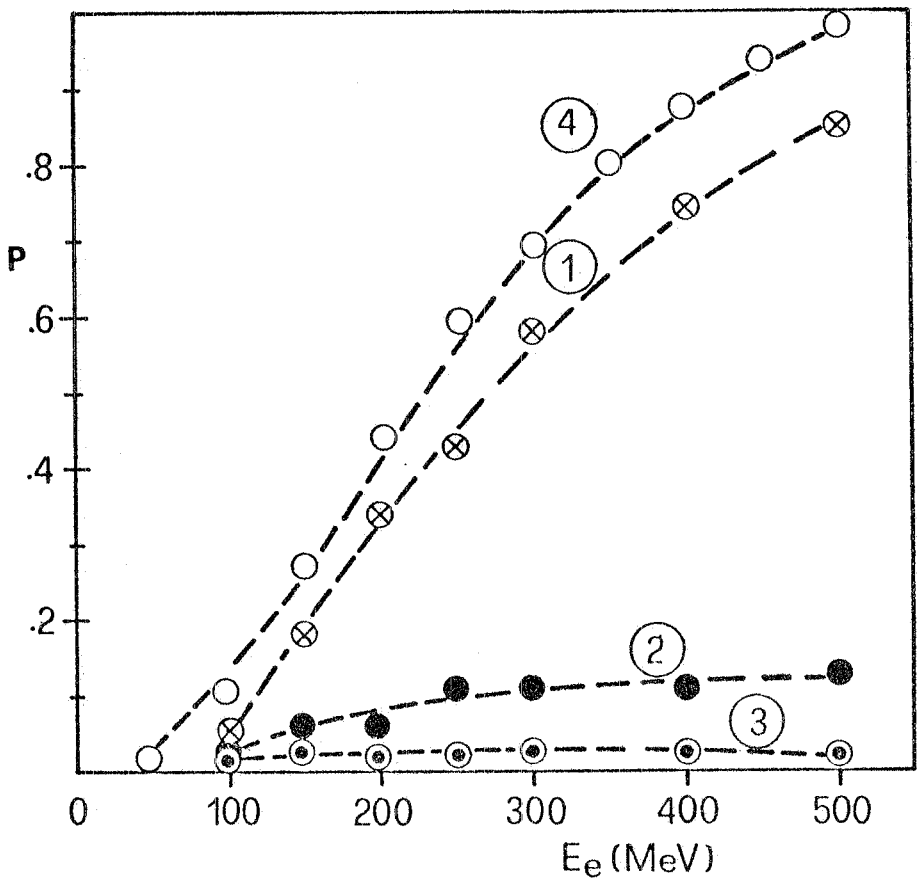

FIG. 3.6 - The probabilities that an electron of energy E_e produce a pulse in counters 2 and 3 and: (1) produces a shower with at least 4 sparks; (2) produces a single track with at least 4 aligned sparks and (3) produces an ambiguous grouping of sparks or a number of sparks less than 4.
The curve (4) is the sum of curves (1), (2) and (3) and represents the probability, P_3, that an electron of energy E_e give a pulse in both counter 2 and 3 (see Fig. 3.3).

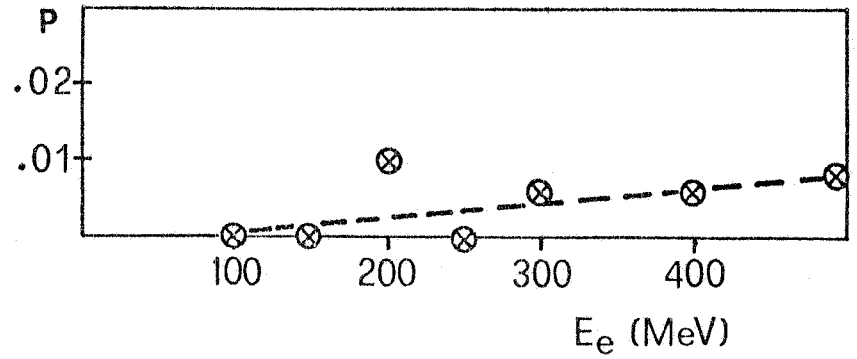

FIG. 3.7 - The probability that an electron of energy E_e give a pulse in counters 2 and 3 and produce in chambers C_2 and C_3 a single track, with at least 6 aligned sparks.

4. - SCANNING AND EVENT SELECTION -

Scanning for events was carried out on projected images of the film enlarged to a size corresponding to $\sim$ 0.2 of the actual one. During the scanning, events were selected by requiring that the associated tracks appear to come from a common point in the e^+e^- interaction region. Tracks in the thin-plate spark chambers C_1, when extended, should come from a common origin within $\pm$ 0.5 cm perpendicular to the beam and $\pm$ 1 cm along the beam direction. Furthermore it was required that the reconstructed vertex of the event coincide, within $\pm$ 1.5 cm, with the beam center in the front view. These limits were set taking into account the average precision in the spatial reconstruction of the events, and the multiple coulomb scattering of the particles along their paths. Of course some e^+e^- events may be lost on the application of these geometrical criteria. The loss, however, was small, being $\sim$ 2% for events having three or more charged particles within the solid angle of the apparatus(x).

Selected events were then classified in the following categories:

a) two-track collinear events if the tracks were collinear within 10^o in both views of the apparatus;

b) two-track non-collinear events, hereafter called 2C events, if the collinearity angle between the tracks was $> 10^o$ in at least one view;

c) events with more than two charged particles detected by the apparatus, i.e. 3C, 4C and 5C events.

Two track collinear events (class a)) can be attributed to the following processes:

(i) Wide angle e^+e^- elastic scattering (WAS events). These events occured at a rate of about 20 per hour, with Adone operating at E = 1 GeV and L $\approx 10^{33}$ cm^{-2} hr^{-1}. They were readily identified by the electromagnetic shower produced along each track in the spark chambers C_2 and/or C_3.(15). Also, as seen in Fig. 3.2, a large pulse height in counters

---

(x) - Even though not essential for the analysis of multi-hadronic events, mention should be made of the fact that for each event selected by the film scanning the information from the "data box" (see Sec. 2), as well as supplementary information relevant for the subsequent analysis, was transferred on computer cards. This supplementary information included: (1) collinearity condition for two-track events; (2) number of tracks, converging in a common point in the e^+e^- interaction region, for multitrack events; (3) behaviour of the detected particles in the thick plate spark chambers C_2 and C_3 ("single track", "shower" - see Sec. 3); (4) presence of correlated tracks and possible stops in the end chambers C_4.

2 and 3 of both telescopes was usually observed. In the present analysis the number of these events was used as a monitor, from which the absolute cross sections of multihadronic production was then deduced. These WAS events served also to determine the frequency distributions of T_{33}, T_{44} and T_{1RF} for e^+e^- collision events and thereby to set fiducial limits to these three time-of-flights to insure the selection of the events due to e^+e^- collisions.

(ii) Muon-pair production: $e^+e^- = \mu^+\mu^-$[23]. These events occurred at a rate of $\sim$ 1/hr for E = 1 GeV and $L \approx 10^{33}$ cm^{-2} hr^{-1}.

Some results on the above electromagnetic two-body processes, i) and ii), have been previously published[15],[23].

(iii) Hadron-pair production. These events were mostly of the type $e^+e^- \rightarrow \pi^+\pi^-$; we have also observed however, one unambiguous case of K^+K^- pair production event as reported at the Cornell Conference[6a]. Results on these hadronic two-body processes will be discussed elsewhere[7b].

Most of the events belonging to class b) were WAS events which had suffered some radiation loss in the initial state(x). Almost all these events appear as complanar with the beam direction, but not collinear[17]. Class b) includes, of course, some multibody final states from e^+e^- interactions, as well as events produced by the interaction of the circulating beam with the gas in the straight section of Adone. This background will be discussed in the following section.

Finally, the multi-body events of class c) are mostly events in which only hadrons are produced. The analysis of this category of events is the principal subject of this paper.

For the selected events belonging to categories b) and c) drawings were made for the two orthogonal views of each event. All details useful for the further analysis of these events, (e.g. large-angle scattering, stopping points, nuclear interactions, etc.), were recorded in these drawings.

(x) - Events with final-state radiation losses are also present in category b, but they are infrequent, since they require, the improbable emission of a hard photon.

5. - BACKGROUND EVENTS. -

During the operation of Adone the pressure of the residual gas in the vacuum chamber was usually about 10^{-9} torr. Part of the machine background was therefore due directly to the interactions of the beams with this residual gas. Additional background events were produced by beam losses and subsequent collisions against the walls of the vacuum chamber. These last background events could be easily recognized by looking at their origin as reconstructed from the corresponding pictures. On the contrary, the former background events could not be distinguished from e^+e^- events because the observed beam-gas collisions occur along the beam and thus in the e^+e^- interaction region. Separation between e^+e^- and spurious events of the former type, therefore, had to be done on a statistical basis. For this purpose, special background runs were interspersed between main runs, at various beam energies. As shall be seen, the contribution of spurious events is appreciable only for the events classified as category b) in the previous section.

The determination of the frequency and types of spurious events was based mostly on background runs in which the machine was operated with a single high-current beam (typically 40 ÷ 60 mA). As a further check, background runs also were made in which Adone operated with both e^+ and e^- beams, but with beam trajectories spatially separated by a few mm so as to eliminate collisions between e^+ and e^- bunches. The events observed in all background runs were studied with the aim of setting criteria that would hopefully improve the signal-to-noise ratio for the multi-hadronic events produced in e^+e^- collisions.

The normalization between the background runs and the e^+-e^- colliding beam runs was based on measurements of small angle electron (or positron) scattering on residual gas nuclei. These measurements were made in both types of runs by using the small-angle-scattering luminosity monitor[18], a drawing of which is shown in Fig. 5.1. Each of the four telescopes $P_iG_iS_i$ is made up of two scintillation counters, P_i, G_i, and a shower counter, S_i. These telescopes are located in such a way as to detect electrons scattered at an angle from 3,5° to 6,1°, as measured from the centre of the colliding region. The shower counter S_i was operated to select high energy electrons, with energy comparable to that of the beam, and to reject lower energy background electrons.

Small angle electron (or positron) gas scatterings were detected by the threefold coincidences $T_i = P_iG_iS_i$, where i = 1, 2 for electrons and i = 3, 4 for positrons.

The following checks were carried out to make it sure that T_i coincidences were essentially due to small angle e^- (or e^+) scattering on residual gas nuclei:

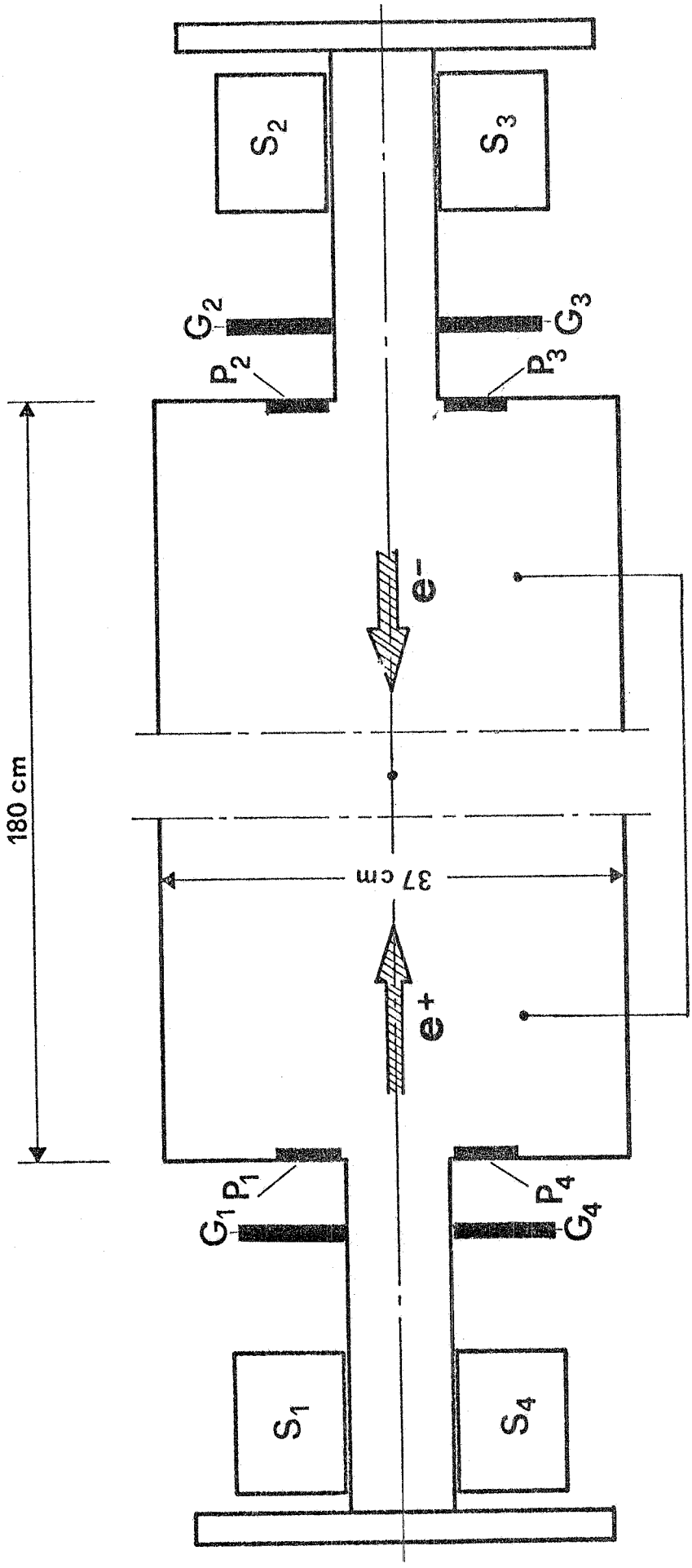

FIG. 5.1 - Monitoring set-up for the luminosity measurement. P_i, G_i(i = 1, 2, 3, 4) are scintillation counters; S_i is a shower counter.

i) T_i was found to be a linear function of both, circulating current and residual gas pressure, as expected for events produced by beam--gas interactions;

ii) with only one e^- circulating beam it was found that $T_{1,4} \gg T_{2,3}$, as expected for small-angle scattering of e^- on nuclei. The reverse (i.e. $T_{2,3} \gg T_{1,4}$) was found to be true when only one e^+ beam was circulating.

Furthermore, when Adone was operated with two colliding beams as in the main runs, (99, 8)% of the counting rates T_i, from a single arm of our monitoring system, were found to be due to beam-gas interactions.

Therefore, these threfold coincidence rates were used to make the normalization between main and background runs.

Background runs were carried out at total energies of 1.5 GeV, 1.9 GeV and 2.1 GeV. On the basis of the normalization procedure outlined above, they were equivalent to $\sim$40%, $\sim$50% and $\sim$75%, respectively, of the corresponding colliding beam runs. No multi-body events of the types 3C, 4C, 5C, were observed at any energy; 2C events were instead observed at a rate depending upon the required penetration depth of secondary particles in each telescope. The trigger employed (M_{mh}, see Sec. 2) implied that at least one particle penetrated to counter 4. The rate of background events depends then on the penetration of the other particle, in the opposite telescope, as indicated in Table 5.1.

It is seen from Table 5.1, that in order to reduce substantially the number of background events, it is convenient to retain only those 2C events in which both particles penetrate to counters 3. Mention should also be made of the fact that a rather large fraction, $\sim$30%, of the background events listed in Table 5.1 contain shower producing electrons.

Of course, since no background event of the types 3C, 4C, 5C was observed, the restriction to reach counter 3, adopted in the analysis of the 2C events, was no longer applied to events with higher visible multiplicity.

TABLE 5.1 - Background events.

2E (GeV)	Number of 2C Events	
	minimum penetration to counter 2	minimum penetration to counter 3
1.5	5	0
1.9	7	1
2.1	22	9

6. - PHENOMENOLOGICAL CLASSIFICATION OF EVENTS -

We recal from Sec. 4 that an "nC" event is a phenomenological classification indicating that n charged particles emanated from a point in the e^+e^- interaction region and were detected by the two telescopes of the apparatus. These events are now to be classified in a more detailed way taking advantage of the calibration measurements discussed in Sec. 3 and the background measurements reported in the previous section. This allows the possible contamination of spurious events to be removed from the multihadron sample.

As a general requirement, all multi-body events had to coincide in space and in time with the collision of the two e^+ and e^- bunches. More precisely it was required, first, that the tracks of any event have their common origin within a fiducial region coinciding with the interaction region. Moreover the event had to occur within a fiducial time region around the instant of beam-beam collision. Both these two fiducial regions were established on the basis of the two corresponding distributions of the WAS events, as outlined in Sec. 4, point (i).

The analysis which follows will be made separately for the 2C events, for 3C events and for 4C and 5C events.

6.1. - 2C-Event Classification. -

Based on the results of the previous sections, a 2C event is defined as an event with only two charged non-aligned tracks, one of which penetrated to counter 4 and the other at least to counter 3 in the opposite telescope. In addition to the two general requirements specified above, it was also required that the time interval T_{33} between the pulses in the two counters 3 should be consistent with that obtained for WAS events. Such a consistency is exibited in the two distributions plotted in Fig. 6.1.

In order to accept a 2C event as a candidate for having been produced in reaction (1) the following criteria were adopted during the analysis. One particle of each 2C event was required

i) to have penetrated to counter 4;
ii) to have given no indication of shower production in either chamber C_2 or C_3;
iii) to have at least 6 aligned sparks along its track, which on the average contain the same number of sparks as the tracks of cosmic ray muons. As seen from Fig. 6.2 this average number is ~ 11. A track with these characteristics will be called a "long track" and indicated by T_L;
iv) the pulse height $H_E(H_I)$, defined in Sec. 2, should be smaller than ~ 1.5 times the value corresponding to a minimum ionizing particle.

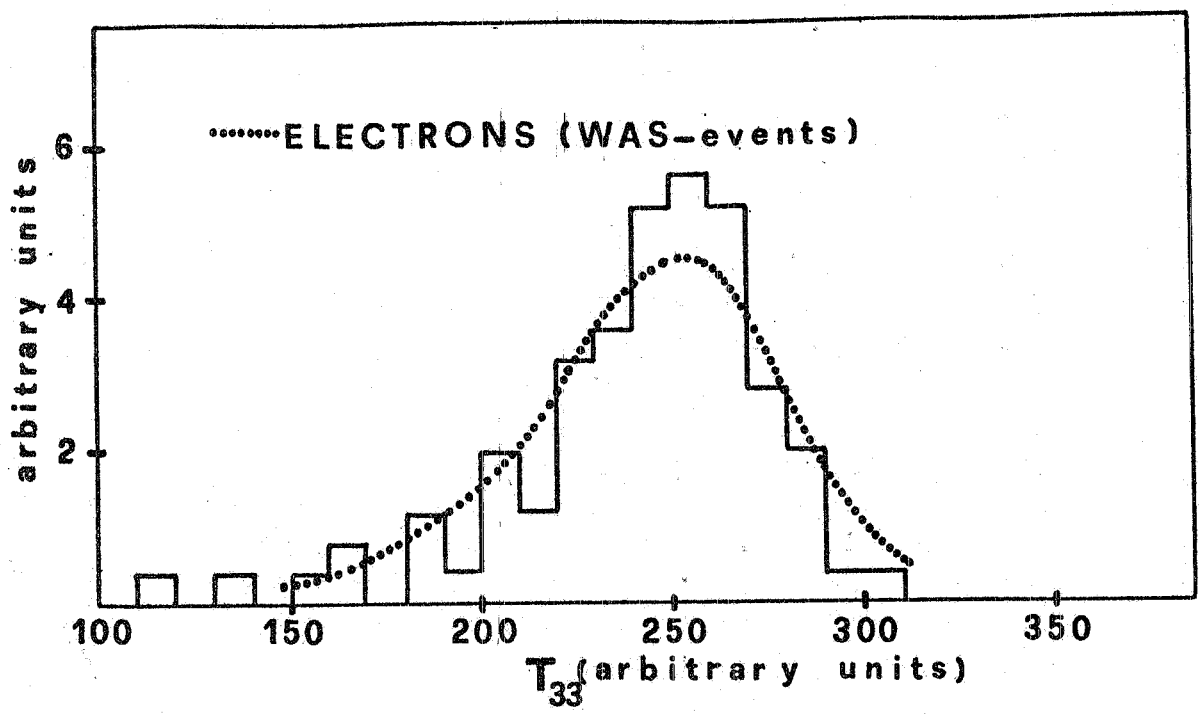

FIG. 6.1 - Distribution of the time of flight between the counters E_3, I_3, T_{33}, for 2C-events. The analogous distribution for e^+e^- (WAS events) is reported for comparison.

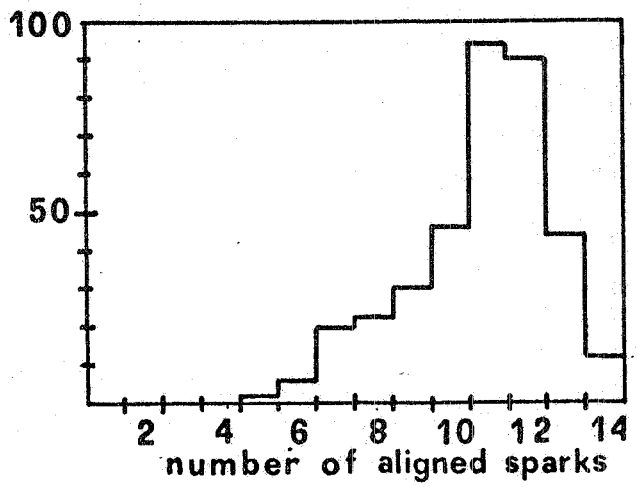

FIG. 6.2 - Frequency distribution of aligned sparks in a penetrating non-interacting hadronic track (T_L), from 2C events.

The pulse-height distribution obtained for a sample of T_L tracks is shown in Fig. 6.3. One sees from this figure that most of the T_L tracks correspond to minimum ionizing particles.

Once a T_L track had been observed in one of the two telescopes, the following possibilities were considered for the behaviour of the other particle, in the thick plate chambers of the opposite telescope:

a) The particle gave a T_L track.
b) The particle produced a single but shorter track (T_S) ending before counter 4. In this case the presence of at least 4 aligned sparks was required in order to define its single track behaviour.

These two possibilities were combined together to define the single track behaviour indicated, in the following, by $T = T_L$ or T_S.

c) The particle produced a well identified electromagnetic shower as defined in Sec. 3 and is indicated in what follows by S.
d) The particle had a behaviour which did not allow unambiguous classification in either category T or S. This case will be indicated by X.

The numbers of observed events having a T_L track in one telescope and either T, S or X behaviour in the apposite telescope, i.e. the numbers with configurations T_L/T, T_L/S and T_L/X, are given in Table 6.1. Data obtained in background runs and normalized as explained in Sec. 5 are also reported in the same table. The last column of the Table contains the numbers of associated WAS events.

One notes that the configurations T_L/S and T_L/X are mainly the result of beam-gas interactions. Also it is seen that the ratio S/X is ~ 2. Considering the results of the calibration measurements reported in Fig. 3.6, one concludes that S and X behaviours are very probably due to low-energy electrons. At the present statistical level of this experiment it seems reasonable to assume that all T_L/S and T_L/X events are due to beam-gas interactions.

The fraction of T_L/T configurations in which one or both tracks are due to electrons can be estimated as follows. The two main non-hadronic processes which might simulate these configurations are:

i) Electron-gas scattering. From the numbers of T/S configurations and the probabilities that an electron simulates a T track, as given in Fig. 3.5, we find that out of the 83 events observed at 2E = 2.1 GeV (Table 6.1), only $\sim$ 2 events should be due to this background process.

ii) e^+e^- scattering (WAS) events, with an angle of non collinearity in excess of 10^o. Since only 7% of all WAS events have non-collinearity angles $> 10^o$ and with the probability of $\sim$ 0.1% that both electrons

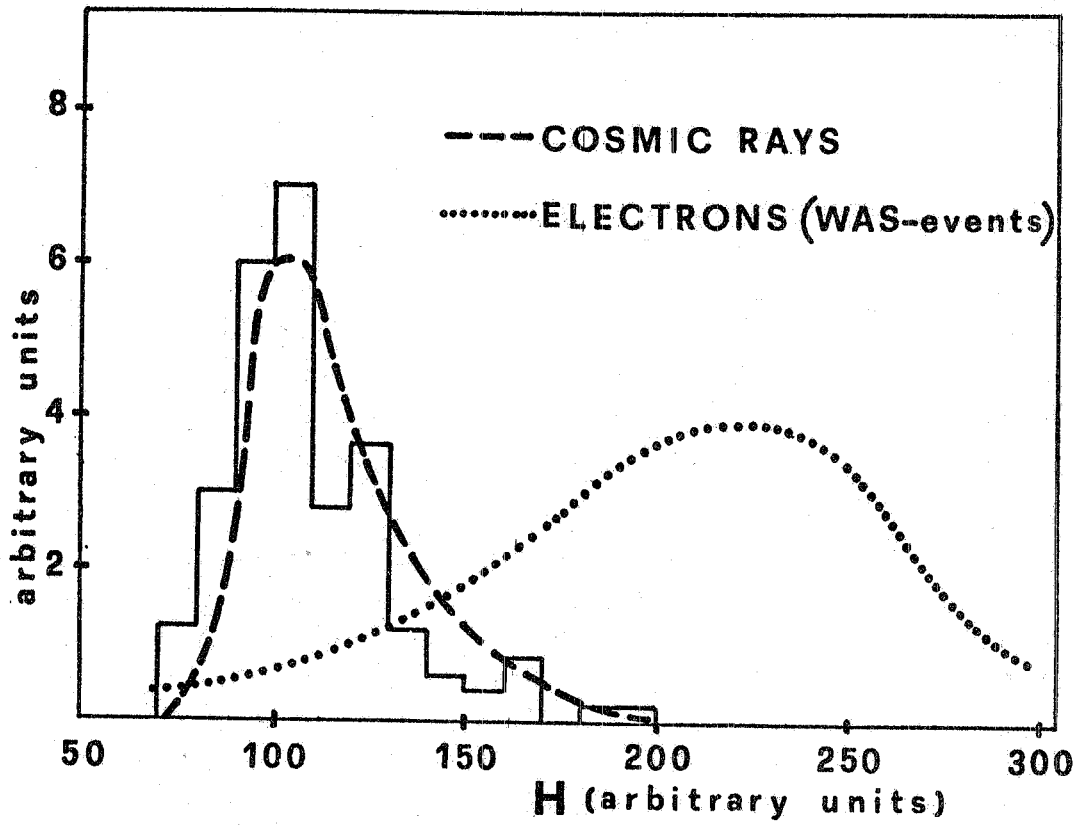

FIG. 6.3 - Pulse height $H_E(I)$ distribution of penetrating hadronic tracks in 2C events compared with cosmic ray and electron distributions.

TABLE 6.1.

Observed configurations in 2C events

2E (GeV)	Type of measur.	Number of 2C events			Number of WAS events
		T_L/T	T_L/S	T_L/X	
1.2	e^+e^-	9	0	0	760
	background	not measured			
1.5	e^+e^-	33	3	2	2419
	background	0	0	0	
1.9	e^+e^-	42	4	2	2112
	background	0	2 ± 2	0	
2.1	e^+e^-	86	12	7	3415
	background	3 ± 2	7 ± 4	3 ± 2	

would appear as T and T_L tracks (Section 3), one finds that ~0.5 event is the expected contribution to the observed T_L/T configurations. Such a contribution will be neglected.

The above discussion shows that the bulk of the T_L/T events cannot be made up of electrons. Evidence for their hadronic nature will be given in the subsequent section in which nuclear interactions in the material of the telescopes are considered. In the discussion that follow T_L/T events will be called 2T events.

6.2. - 3C-event classification. -

We recall that the master coincidence M_{mh} implied the penetration of at least one particle up to counter 4 of one telescope, and up to counter 2 for a particle in the opposite telescope. Thus every multibody event contained at least one "long track" T_L (Sec. 6.1) and at least one track reaching counter 2 of the opposite telescope.

A total of 266 3C events were observed in e^+e^- collisions at all energies. However no 3C event was observed during background runs with a single beam or two non colliding beams. The great majority of these events, 245, contained two single tracks, one of which was a T_L track. Twenty of the remaining events had characteristically only one clear single track (usually a T_L track) and in one event three showers were observed. These latter 21 events will not be considered further in this paper.

It is important to estimate the fraction of 3C events containing electrons and, therefore, not due to the multi-hadronic reaction (1). This estimate has been made starting from the seven T_LTS events in which one shower was observed. Using the results of the calibration measurements reported in Fig. 3.6 and assuming pessimistically that all observed showers are produced by 100 MeV electrons we found that the above fraction is only about 1% of the 3C events. This percentage is over-estimate, since some of the events with showers may well be due to pion charge exchange. The very small number of electrons as final state particle is also consistent with the observations on pulse height in counters 2 and 3, when only one particle is seen to traverse them in a telescope. This pulse height distribution results to be very similar to that for cosmic ray muons and not for electrons.

The number of 3C events of the type T_LTT (≡ 3T) observed at each total energy 2E are given in Table 6.2.

6.3. - 4C and 5C event classification. -

During the search for multihadron events no events having more than 5 charged secondaries were observed.

As no 4C or 5C event was observed during the background runs, all observed e^+e^- events were included in this sample.

In analysing these events, no secondaries were seen to appear as showers. Considering the results on 3C events and the reduced number of 4C and 5C events, we have taken all secondaries to be hadrons. The number of the events, which have been called 4T and 5T, observed at the various total energies 2E are given in Table 6.2.

6.4. - Auxiliary observations on multi-particles events. -

Electromagnetic showers produced by photons also were observed in multi-body events by their conversion before or in chambers 2 and 3. These showers were not associated with charged particles of the event, as specified by the requirement (Sec. 3) of observing the non-aligned sparks within a 15^{o} cone around each track direction. In most cases the direction of the photon could only be roughly established by observation of the shower produced. As no such shower was observed among events of the type $e^{+}e^{-} \rightarrow \mu^{+}\mu^{-}$ or from cosmic ray runs, the photon conversions observed in multi-hadron events have been assumed to originate from decays of neutral pions produced in these events.

In some cases showers also were observed in chambers C_1. They presumably originated in the wall of the vacuum chamber of the machine. These showers could have been produced by secondary electrons; however, we recall that the number of secondary electrons, particularly in 3C, 4C and 5C events, is very small ($< 1\%$ of all tracks in 3C events). Consequently, all showers observed in chambers C_1 associated with multiparticle events, were attributed to photons from π^{o} decay.

Additional information concerning the multibody events was given by counters A and B. The pulses from these counters were in fact recorded in the data box mentioned in Sec. 2, when they occurred in coincidence with the master trigger M_{mh}.

A summary of the numbers of events with associated γ and/or pulses from counters A, B is given in Table 6.3 for the different multihadronic events 2T, 3T, 4T observed at various energies (2E).

It was found that in 2÷3% of the cases, the collinear VAS events were accompanied by spurious signals of either counters A, B. Accordingly, the numbers of events with A or B signals reported in Table 6.3 have been corrected for this small background contamination.

The usefulness of the supplementary information related to the presence, in the recorded events, of γ and/or A, B signals, will be made clear in Sec. 10.

TABLE 6.2

Summary of results on more-than-two charged-particle events.

2E (GeV)	WAS events	3T	4T	5T
1.2	760	3	0	0
1.5	2419	38	14	1
1.65	992	17	8	0
1.9	2164	35	10	1
2.1	6187	122	39	6
2.4	1101	23	13	4

TABLE 6.3

Events associated with a γ and/or signals in counters A and B(x)

Total energy 2E (GeV)	WAS	Number of events of the type					
		2T + γ	2T+A or B	3T + γ	3T+A or B	4T + γ	4T+A or B
1.2	760	0	0	0	0	0	0
1.5	2419	4	7	8	9	1	0
1.9	2164	15	7	11	12	1	0
2.1	6187	14	22	30	28	2	11
2.4	1101	--	--	8	5	3	1

(x) - A small fraction of the events reported in the Table, contained indeed more than one γ and/or both signals from counters A, B.

7. - NATURE OF SECONDARY PARTICLES AND REACTIONS -

The criteria adopted in the selection of events as described in the previous section assured that secondary particles were singly charged and penetrating, and were improbably electrons. Qualitatively these particles also were seen to give rise to nuclear interactions and wide angle scatterings. The effective experimental interaction-length for nuclear interactions was estimated by determining the fraction of secondary particles from multi-body events which did interact in the telescopes.

In order to compare our results with those from counter experiments on pion-nucleus interactions, an interaction was defined as a stop of a track, with or without secondary tracks, when all penetrating secondaries had angular deviations of more than 25°. Thus, wide angle scatterings ($> 25^{o}$) also were included as interactions. Averaging over the apparatus, the experimental absorption length in Iron for the secondary particles from multiparticle events was found to be 114 ± 12 g/cm^2. This value is $\sim$ 1.2 times the geometric interaction length for Iron and is in good agreement with experimental values measured in counter experiments[25], when averaged over the assumed pion energy spectrum(x).

Moreover for 2T events, where the statistics are sufficiently high to make a more detailed comparison possible, the distribution of the interactions as a function of absorber depth is compared with other similar spark chamber results[26] in Fig. 7.1. The latter were obtained with 450, 500 and 600 MeV/c pions incident on Iron-plate spark chambers. The agreement between the distributions is considered satisfactory also on account of the extended energy spectrum and slight differences in the criteria followed to identify interactions.

The above results show that the secondaries of the multi-particle events observed are mostly hadrons, with nuclear interaction characteristic consistent with those observed for pions having a kinetic energy of $\sim$ 350 MeV. This conclusion is in line with and reinforces the conclusions of Sec.'s 6.1 and 6.2, that most of final-state particles in the multiparticle events are not electrons. It will be assumed in what follows that all multi-hadronic events selected according the criteria discussed in Sec. 6, and reported in the Tables 6.1, 6.2 and 6.3, contain only pions in their final states. This assumption is supported by the results from $p\bar{p}$ annihilations, which also have a center-of-mass energy of $\sim$ 2 GeV and which recorded $\sim$ 95% of the final states as containing pions[27]. Further suggestions along this same line are given by the low K/π ratio found in the high energy hadronic interactions[28].

(x) - This spectrum was obtained from the Montecarlo simulation of the experiment, which is described in Sec. 8.

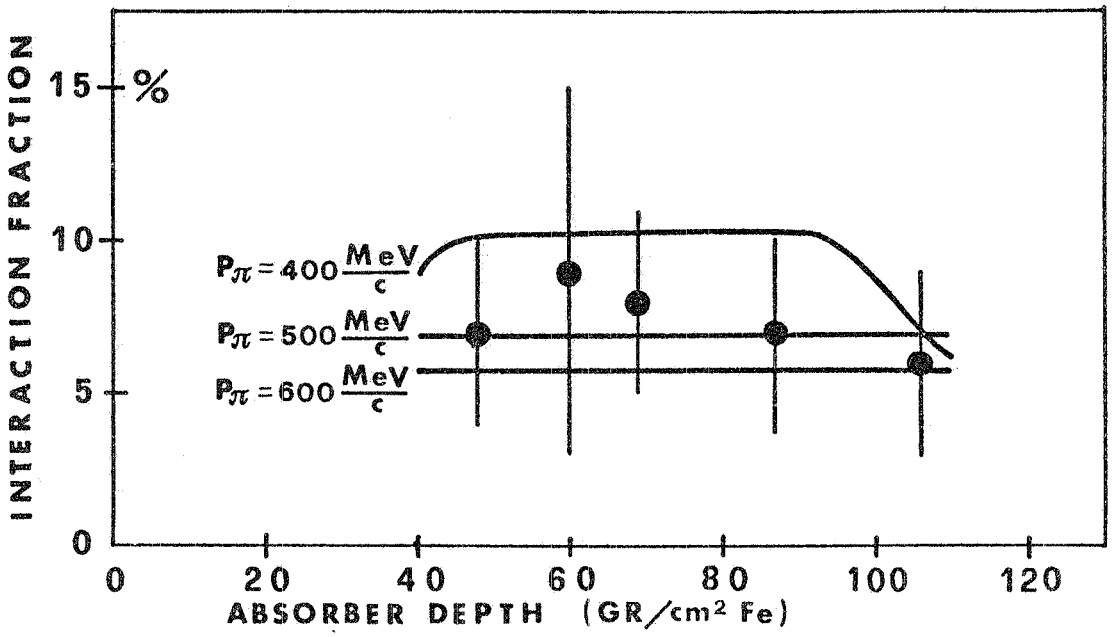

FIG. 7.1 - Distribution of nuclear interactions in 2T events as function of absorber depth. Calibration curves from ref. (26) are indicated for 3 different pion momenta.

Charged pion production infers of course also the production of neutral pions. Analysis based on Montecarlo estimates of the number of converted gamma rays for the event types 2T, 3T and 4T indicates, when compared with experiment (see Table 6.3) that the average numbers of π^o produced is ~ 2 in each reaction.

Based on these observations, the following reactions have been considered as the major contributors to the multi-particle events reported here:

$$e^+e^- \longrightarrow \begin{cases} \pi^+\pi^-\pi^o & (4) \\ \pi^+\pi^-\pi^o\pi^o & (5) \\ \pi^+\pi^-\pi^+\pi^- & (6) \\ \pi^+\pi^-\pi^+\pi^-\pi^o & (7) \\ \pi^+\pi^-\pi^o\pi^o\pi^o & (8) \\ \pi^+\pi^-\pi^+\pi^-\pi^o\pi^o & (9) \\ \pi^+\pi^-\pi^+\pi^-\pi^+\pi^- & (10) \end{cases}$$

The limit of six pions in the final state is a reasonable hypothesis since the fraction of $p\bar{p}$ interactions at rest with more than six pions is $\lesssim 10\%$[27], and since, as pointed out previously, the average number of π^o's produced is $\lesssim 2$ even for 4T events. Also the cross section deduced using a Montecarlo simulation with the above reactions, results in a falling cross section with increasing number of pions in the final state (see Fig. 10.9 later). Finally, it should be noticed that, if multi-

plicities higher than a maximum value of 6 were introduced in the analysis, the information on the reactions involved would become less significant on account of the greater number of channels, with the same data. Thus ignoring the rather small contributions from multiplicity states higher than 6, introduces less uncertainties in the resulting partial cross sections than including them.

8. - MONTECARLO SIMULATION OF THE EXPERIMENT -

A Montecarlo program was written to simulate the experiment and to calculate the efficiencies for detection of final states with more than two charged particles. In these calculations particles were generated according to phase space and according to the reactions listed in the previous section. Events for a particular final state were randomly generated along the beam line, with a distribution which took into account the finite length of the source. The secondary charged particles and gammas from π^0 decay were then traced through the vacuum chamber wall and through the spark chambers and counters of the apparatus.

From these calculations the following information was obtained:

i) efficiency for the detection of a given final state;

ii) frequency of detected events with a pulse in counter A or B, due to a charged particle or to a γ from π^0 decay converted in the wall of the vacuum chamber;

iii) frequency of electromagnetic showers produced by neutral pions associated with detected events.

In the calculations of the detection efficiency, the nuclear interactions of pions was taken into account by using the results of attenuation measurements in various materials as reported by different authors[25]. The attenuation cross section used in the computations in shown in Fig. 8.1[x]. These cross sections are for pion-nucleus (Fe) collisions in which a penetrating secondary is scattered at an angle greater than 25^o. For materials other than Iron their cross section were scaled by $A^{2/3}$. No account was taken of small effects such as $\pi - \mu$ decay, or multiple coulomb scattering.

For each gamma ray from π^0 decay, the conversion point along the direction of motion in the apparatus was randomly selected along an exponential, measured in conversion lenghts. The asymptotic value of the conversion length at high energy was used. After conversion, the shower was followed as if it were a single particle, for a depth corresponding to the average penetration of a shower of that energy. The penetration as a function of energy was deduced using the results of the calibration measurements reported in Sec. 2, as well as results by other authors[29].

(x) - Details can be found in ref. (25).

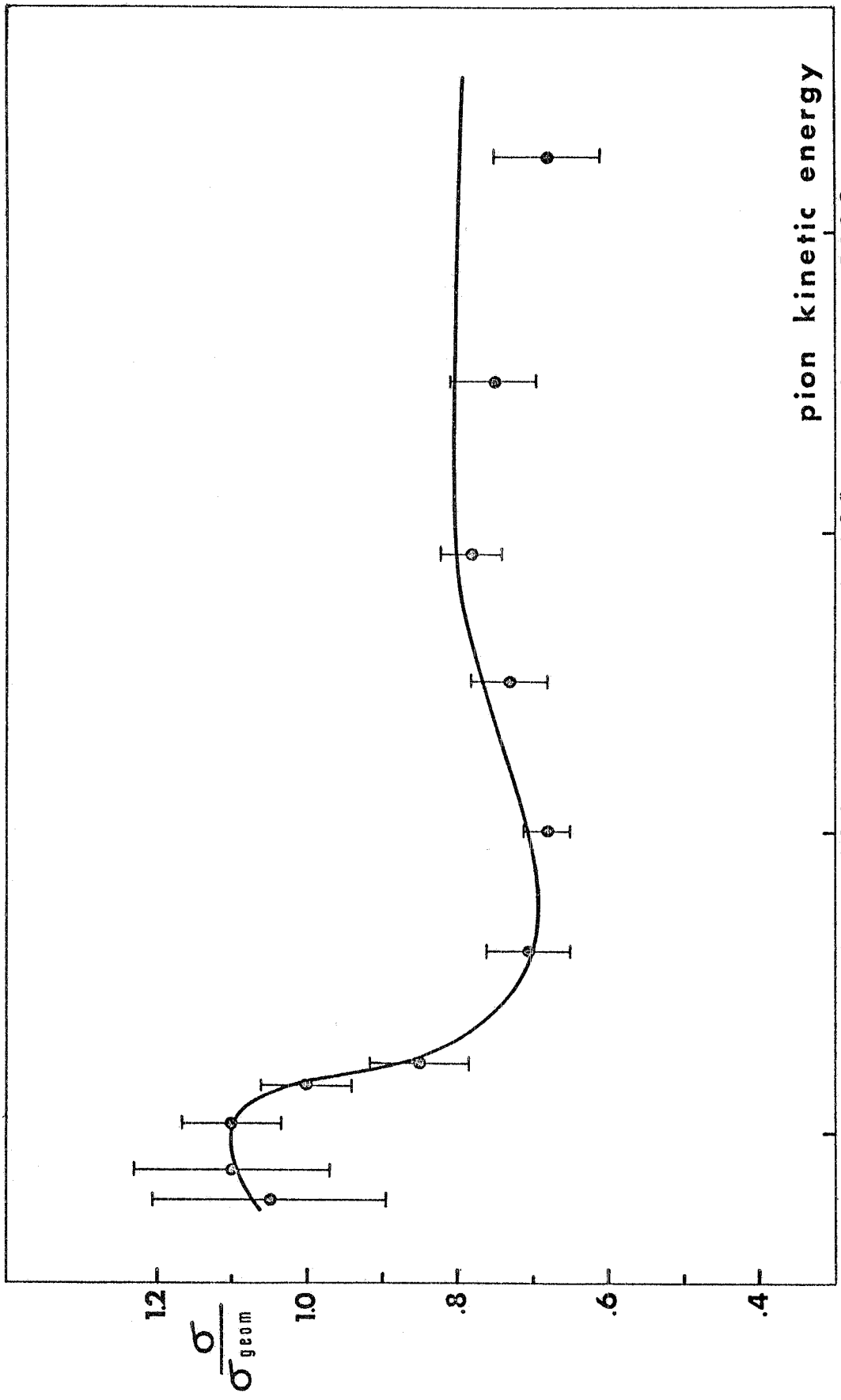

FIG. 8.1 - Nuclear attenuation cross section in Iron as function of pion kinetic energy, used in the Montecarlo simulation of the experiment.

Dynamic factors for each event were used only in the generation of three-body final states ($\pi^+\pi^-\pi^o$). The factor used was $\sin^2\Theta\ \sin^2\vartheta$[1] where ϑ is the angle between the e^+e^- beam direction and the normal to the production plane, and Θ is the angle between the two charged pions in that plane.

The values obtained for the detection efficiencies are in the range of $\sim$ 1% ÷ 7% and vary with the reaction, detection configuration, and total energy 2E. These are shown for the most probable configurations in Fig. 8.2. Low values of the efficiencies are found, essentially because of the relatively small solid angle of the two telescopes ($\Omega/4\pi \approx 0.2$) and because of the losses due to nuclear or range absorption of the produced pions.

The errors in the efficiencies are between 10 and 20% for most reactions and are principally due to the statistical accuracy in the computation.(x) For those reactions with lower efficiencies ($\sim$ 1%), the error increases to $\sim$ 30%.

The sensitivity of the calculated efficiencies to changes in the mean free path λ_c has been estimated to be approximately equal, i.e.

$$\Delta\varepsilon/\varepsilon = \sim \Delta\lambda_c/\lambda_c$$

As stated before, a statistical production mechanism was assumed in all the quoted calculations. The results that would be obtained by assuming different production mechanisms, e.g. $e^+e^- = A_1^{\pm}\pi^{\mp} = 2\pi^+ + 2\pi^-$; $e^+e^- = \rho^o\varepsilon^o = 2\pi^+ + 2\pi^-$; $e^+e^- = \rho^o\pi^+\pi^-$, etc., will be discussed elsewhere[30].

(x) - For every reaction (4) ÷ (10) about 2×10^4 events were randomly generated.

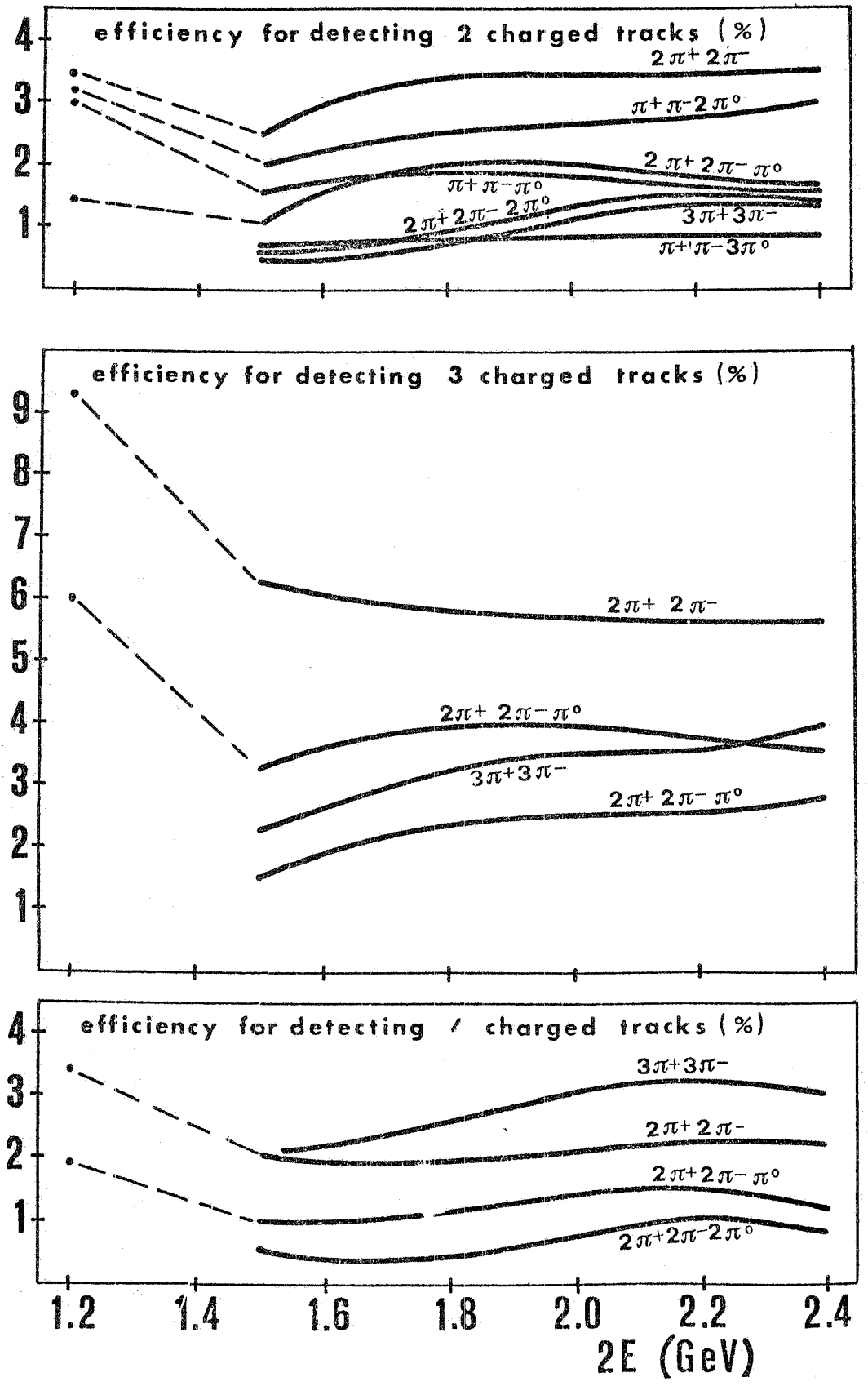

FIG. 8.2 - Efficiencies to detect in various configurations processes with different final states, vs. 2E. Efficiencies have been computed taking in account only invariant phase space. The point at 2E = 1.2 GeV had different triggering condition.

9. - THE REACTION $e^+e^- \rightarrow \pi^+\pi^-\pi^+\pi^-$ FROM ANALYSIS OF 4T EVENTS. -

From the events classified as 4T, it is possible by the procedure discussed below, to determine, the number of those containing only four charged hadrons. As indicated earlier (Sec. 7), we will assume that all secondaries are pions. i.e. that these special 4T events belong to the reaction $e^+e^- \rightarrow \pi^+\pi^-\pi^+\pi^-$ (6). Of course 4T events of this type were searched for among those which had no associated γ (Sec. 6.4), or pulses present in counters A or B.

The angles in both views for each track were measured and the space angles calculated. Using these angles as particle directions, the four equations resulting from the conservation of four-momenta were solved to obtain the momentum of each particle. The error in the projected angles was $\sim \pm 2^o$, due to multiple Coulomb scattering in the vacuum chamber walls and measurement errors. This error produces an average uncertainty of $\pm$ 10 MeV/c in the calculated momentum. The solution was considered as valid if all momenta were positive and consistent with the penetration depth of each particle in a telescope.

Although all 4-pion events were identified by the above method, events with five or more pions, of which only four were detected by the apparatus, could give a background contribution to reaction (6) by simulating 4-pion events. In order to determine this background contamination, events with five and six pions were generated using the Montecarlo program described in the previous section. Those that gave an allowed trigger and only four charged particles in the telescopes, were analysed in the same way as 4T events. The fractions of events that gave a good fit as a 4-pion event, were 12% for $\pi^+\pi^-\pi^+\pi^-\pi^o$ final states and 18% for $\pi^+\pi^-\pi^+\pi^-\pi^{\pm}\pi^{\mp}$ final states. The percentages given above were found to be essentially independent of the total center of mass energy, 2E.

The results of this special analysis are given in Table 9.1. The number of associated WAS events is given (column 2) for each energy at which events were analyzed. The number of 4T-events with no associated γ or pulses from counter A or B is called N_{4T} (column 3). In column 4 are the numbers of "reconstructed 4T-event" ($N_{4T\text{-reconst.}}$); i.e. events which were kinematically consistent with the hypothesis of only 4 pions in the final state. The actual numbers of 4π-events, $N_{4\pi}$, were obtained by subtracting the background of fake 4π-events due to 5π- and 6π-events from $N_{4T\text{-reconstr.}}$ For the sake of completeness the numbers of 4T-events with associated γ and/or signals from counters A or B also, are listed in the last column of Table 9.1.

The cross section for process $e^+e^- \rightarrow \pi^+\pi^-\pi^+\pi^-$ calculated from the numbers of $N_{4\pi}$ has been previously reported(13).

TABLE 9.1

2E (GeV)	WAS	N_{4T}	$N_{4T\text{-RECONST.}}$	$N_{4\pi}$	$N_{(4T+\gamma)} + N_{(4T+A \text{ or } B)}$
1.2	760	0	0	0	0
1.5	2419	12	11	11	1
1.65	992	8	6	6	0
1.9	2164	8	5	5	1
2.1	6187	13	9	6	13
2.4	1101	5	2	1	4

These results show an enhancement of the cross section around 2E = ~ 1.6 GeV, (see Fig. 10.2), suggesting the possible production of a ζ'-meson ($M_{\zeta'} = \sim 1.6$ GeV, $\Gamma_{\zeta'} = \sim 350$ MeV. The interpretation of the results reported in this Section will be further discussed in Sec.s 10 and 11.

10. - ANALYSIS AND RESULTS -

The objective of this section is to describe the methods used in obtaining partial cross sections for the reactions (4) to (10). The input data to these calculations are the observed numbers of 2T, 3T, 4T and 5T events, with and without converted photons and pulses in counters A and B. Also utilized are the efficiencies, as determined in Section 8, for each reaction to contribute to these observed configurations.

As mentioned previously (Sec. 5), most the multiparticle events are observed with little if any background.

This is particularly true for 3T, 4T and 5T events; however, for 2T events this was only true when the criteria on track penetration were used to suppress gas-beam interactions (see Sec. 5). A further correction to the number of 2T events also was necessary due to several well known processes, i.e.

(11) $e^+e^- \rightarrow \mu^+\mu^-\gamma$, and $\pi^+\pi^-\gamma$

(12) $e^+e^- \rightarrow e^+e^-\mu^+\mu^-$, and $e^+e^-\pi^+\pi^-$

The small number of these events that were detected by our apparatus was estimated[31] (a total of 16 2T events) and accordingly a correction applied.

The calculation of the partial reaction cross sections was made by solving the following system of k equations at each energy, 2E:

$$N_K = \mathcal{L} \sum_A \varepsilon_K^{(A)} \cdot \sigma_A \tag{13}$$

where A = 1, 2, ... 7 indicates one of the seven reactions (4) ÷ (10), listed in Sec. 7;
K = 1, 2, ... 11 is one of the eleven observed configurations, listed in the first row of Table 10.1 (2T, . . . 5T configurations);
N_K is the number of events in the configuration K;
σ_A is the cross section of process A;
$\varepsilon_K^{(A)}$ is the efficiency for detecting process A in the configuration K;
$\mathcal{L}$ is the integrated luminosity.

A standard Monte-Carlo method was applied in solving these equations. Taking into account statistical errors for N_K and $\varepsilon_K^{(A)}$, a random search for a χ^2 minimum was made over a range for σ_A from

TABLE 10.1

Summary of the numbers of the collected events for each type.

2E (GeV)	$\mathcal{L}$ (10^{+33} cm^{-2})	NUMBER OF EVENTS IN THE FOLLOWING CONFIGURATIONS(x)										
		2T (Total)	2T + γ	2T+A or B	3T (Total)	3T + γ	3T+A or B	4T (Total)	4T+γ	4T+A or B	$N_{4\pi}$	5T
1.2	5.07	9	0	0	3	0	0	0	0	0	0	0
1.5	23.8	33	4	7	38	8	9	14	1	0	11	1
1.65	19.5	--	-	-	17	-	-	8	-	-	6	0
1.9	43.5	42	15	7	35	11	12	10	1	0	5	1
2.1	163.0	83	14^	22^	122	30	28	39	2	11	6	6
2.4	49.7	--	--	--	23	8	5	13	3	1	1	4

(^) - The integrated luminosity corresponding to these categories of events was $\mathcal{L} = 90 \times 10^{33}$ cm^{-2}.

(x) - Some numbers of events are missing because of insufficient background measurements or reduced efficiency of the spark chambers to recognize showers.

0 to 100 nb. χ^2 values which did not exceed 1.2 times the number of equations were considered as valid solutions. The average value and variance for each σ_A were determined from the distribution of values satisfying the above χ^2 criterion.

In principle it is possible to solve these equations at each energy and, in general, this was done. However, due to the lack of some information at certain energies, this was not always possible.

The discussion which follows attempts to explain the results as they appear in Table 10.2, where the quoted statistical errors correspond to one standard deviation.

i) When solving equations (13) the measured fractions $(3T+\gamma)/3T$ and $(4T+\gamma)/4T$ are the leading quantities in separately determining the cross sections $\sigma(2\pi^+2\pi^-\pi^o)$ and $\sigma(2\pi^+2\pi^-2\pi^o)$. The accuracy of such a separation depends on the precision with which the above fractions and the average π^o detection efficiency of our apparatus are known. Consequently, at energies where for any reason γ's were not detected, it is only possible to give the cross section for the sum of the two processes, i.e. $\sigma_{4c+n} \equiv \sigma(2\pi^+2\pi^-\pi^o)+\sigma(2\pi^+2\pi^-2\pi^o)$. In these cases a systematic error, appearing in the parenthesis, was given. It was taken to correspond to the two extreme possibilities of considering only one of the two processes to be present at a time.

ii) The cross section $\sigma(2\pi^+2\pi^-)$ can be calculated in two substantially different ways.

1) From the number of events with only four pions, $N_{4\pi}$, as deduced in Section 9 and given in Table 9.1.

2) By an over-all fit of all data , i.e. by solving equations (13). This latter method was applied by solving these equations both, with and without the equation referring to $N_{4\pi}$.

All results obtained by these different methods agree, within the errors, showing the internal consistence of our data. The results in Table 10.2, column 3 (see also Fig. 10.2) are those derived by this method. At the total energy 2E = 1.2 GeV the error values, appearing in parenthesis in Table 10.2, give the limits for $\sigma(\pi^+\pi^-\pi^+\pi^-)$ and σ_{4c+n} when one assumes that all observed 3T events or none were produced by these channels. At 2E = 1.5 GeV the error in $\sigma(\pi^+\pi^-\pi^+\pi^-)$, appearing in parenthesis, depends on the fit procedure; it reflects the fact that the channel $\pi^+\pi^-\pi^+\pi^-\pi^o$, whose cross section $\sigma(\pi^+\pi^-\pi^+\pi^-\pi^o)$ is at this energy compatible with zero, can be included or not in the calculations.

TABLE 10.2

Summary of the cross sections.

2E (GeV)	σ_{2c+n}	$\sigma(\pi^+\pi^-\pi^+\pi^-)$	$\sigma(\pi^+\pi^-\pi^+\pi^-\pi^o)$	$\sigma(\pi^+\pi^+\pi^+\pi^-\pi^o\pi^o)$	σ_{4c+n}	$\sigma(\pi^+\pi^-\pi^+\pi^-\pi^+\pi^-)$	$\sigma_{\geq 4c}$	σ_{tot}
1.2	$(30\pm2)\pm15$	$(3\pm3)\pm3$			$(5\pm5)\pm6$	<1	$(8\pm2)\pm6$	$(38\pm4)\pm16$
1.4							31 ± 15	
1.5	$(30\pm4)\pm11$	$(18\pm3)\pm3$	6 ± 7	16 ± 8	22 ± 7	3 ± 3	43 ± 9	$(73\pm4)\pm9$
1.65		23 ± 11			$(18\pm4)\pm9$	<3	$(41\pm4)\pm10$	
1.77							24 ± 10	
1.9	$(22\pm5)\pm4$	5 ± 2	5 ± 3	7 ± 3	11 ± 3	3.5 ± 1.5	19 ± 3	$(44\pm4)\pm4$
2.0							21 ± 11	
2.1	$(25\pm6)\pm3$	1.5 ± 1.0	9.5 ± 3.0	3 ± 2	12 ± 3	3.5 ± 1.0	16 ± 3	$(45\pm9)\pm3$
2.4		<4	10^{+7}_{-4}	3 ± 4	13 ± 4	4 ± 2	16 ± 4	

Definitions used in the table are, as follows:

$\sigma_{2c+n} = \sigma(\pi^+\pi^-\pi^o) + \sigma(\pi^+\pi^-\pi^o\pi^o)$

$\sigma_{\geq 4c} = \sigma(e^+e^- \rightarrow$ at least 4 charged $\pi)$

$\sigma_{4c+n} = \sigma(\pi^+\pi^-\pi^+\pi^-\pi^o) + \sigma(\pi^+\pi^-\pi^+\pi^-\pi^o\pi^o)$

$\sigma_{tot} = \sigma(\pi^+\pi^-$ + anything).

Where two errors are reported the first, in parenthesis, is the systematic one and the second is the statistical error.

iii) Many channels produced in the e^+e^- interactions are of the type

$$e^+e^- \longrightarrow \pi^+\pi^- + n\pi^o, \text{ with } n \gtrsim 1$$

and contribute, therefore, to the same $2T + \gamma$ configuration(x). The information which can be derived from the observed $2T + \gamma$ events is consequently insufficient to separate the various contributions. Nevertheless the observed fraction $(2T + \gamma)/2T$ is small enough to exclude contributions in excess of $\sim 30\%$ from channels with $n \gtrsim 3$, at any energy. In evaluating the cross-section $\sigma_{2c+n} \equiv \sum_n \sigma(\pi^+\pi^- + n\pi^o)$ these contributions have not been considered, so that.

$$\sigma_{2n+c} = \sigma(\pi^+\pi^-\pi^o) + \sigma(\pi^+\pi^-\pi^o\pi^o)$$

The numerical, value of σ_{2c+n} reported in column 2 of Table 10.2, is obtained by taking as detection efficiency the average value

$$\bar{\varepsilon} = \frac{1}{2}\left[\varepsilon_{2T}(\pi^+\pi^-\pi^o) + \varepsilon_{2T}(\pi^+\pi^-\pi^o\pi^o)\right].$$

Also in this case, as in the case of σ_{4c+n} considered above, the limits of the quoted systematic error (appearing in the parenthesis) correspond to assuming only one of the two reactions present at a time. Precisely it is found that the lower limit correspond to considering only process $e^+e^- \longrightarrow \pi^+\pi^-\pi^o\pi^o$.

It should be pointed out that experimental information from the "$\gamma\gamma$ group"(12), as well as theoretical considerations by various authors(+), suggest that at Adone energies the contribution from the $\pi^+\pi^-\pi^o$ channel to the (2c+n)-cross-section is at most a few nanobarn. Assuming that $\sigma_{2n+c} \sim \sigma(\pi^+\pi^-\pi^o\pi^o)$ is, therefore, most probably correct.

(x) - It should be recalled (see Table 6.3) that the configurations $nT + \gamma$ in a few cases involve the presence of more than one detected γ. For example, the $2T + \gamma$ configuration involves two identified γ in a fraction of cases which is less than 10%. The statistical significance of this additionnal information is too poor to be exploited in the analysis, and consequently was ignored.

(+) - See, for instance, J. Layssac and F.M. Renard - Lett. Nuovo Cimento 1, 197 (1971).
Essentially these considerations are based on the hypothesis that process $e^+e^- \longrightarrow \pi^+\pi^-\pi^o$ is dominated by the ω or ϕ tail; an hypothesis which appears to be valid up to 2E= 1 GeV according to ACO data(3b).

The results given in Table 10.2 are also shown in graphical form in the Fig.s from 10.1 to 10.8. Available data from other Laboratories[3b][32] and/or from other groups working at Adone[11][12] also have been reported in the figures, with the purpose of extending the information, in particular towards lower energies(x). All these results will be shortly discussed in the next section. We add here that, the systematic errors (given, in our case, in parenthesis in Table 10.2) are indicated by open boxes throughout the figures. In the case of our data the meaning and the method of estimating systematic errors has been specified above. It should be noticed that these errors do not include the uncertainties in the integrated luminosity, $\mathcal{L}$, and in the calculated efficiencies, $\varepsilon_K^{(A)}$. A few doubtful events which were disregarded in the course of our analysis (see Sec. 6) could also represent an additional source of error, via N_K. We estimate, however, that errors such as the above which have been neglected in any case do not exceed the quoted statistical errors; the latter involving, as mentioned already, statistical uncertainties in both, $\varepsilon_K^{(A)}$ and N_K.

It is worthwhile to observe that there is substantial agreement between the results obtained by the various groups working at Adone, as reported in the previous figures. One noteworthy discrepancy is found for σ_{tot} (fig. 10.8) in the region of 2E = 2 GeV, where the $\gamma\gamma$-group value appears to be somewhat lower than the values measured by the other groups. Slightly lower values are found also, by the same group, for the σ_{2c+n}, showed in fig. 10.1, where the points from the $\gamma\gamma$-group have been computed assuming that n = 1, 2, 3, 4. On the other hand, as pointed out already, the lower limit of σ_{2c+n} within the systematic errors given in Fig. 10.1, corresponds to channel $e^+e^- \longrightarrow \pi^+\pi^-\pi^o\pi^o$. This is the minimum cross-section we can give, since any mixture of states with a number of π^o's from 1 to 4 would increase the value of σ_{2c+n}. Hence there seem to be a systematic difference between the cross sections measured by the two groups. We do not believe, however, that a great significance can be attached, at present, to these apparent discrepancies on account not only of possible neglected systematic uncertainties, but also of the differences in the hardwares employed in the experiments (differencies in angular acceptance, energy cut-offs, etc.).

We report in Fig. 10.9 the total cross section, at 2E = 2.1 GeV, as a function of the total number of final state pions (charged plus neutrals). The multiplicity curve has been given explicitely only at this

---

(x) - Values of the cross section $\sigma_{\geq 4c}$ obtained from a re-analysis of data previously reported by Barbiellini et al.[33] are also given in Fig. 10.7.

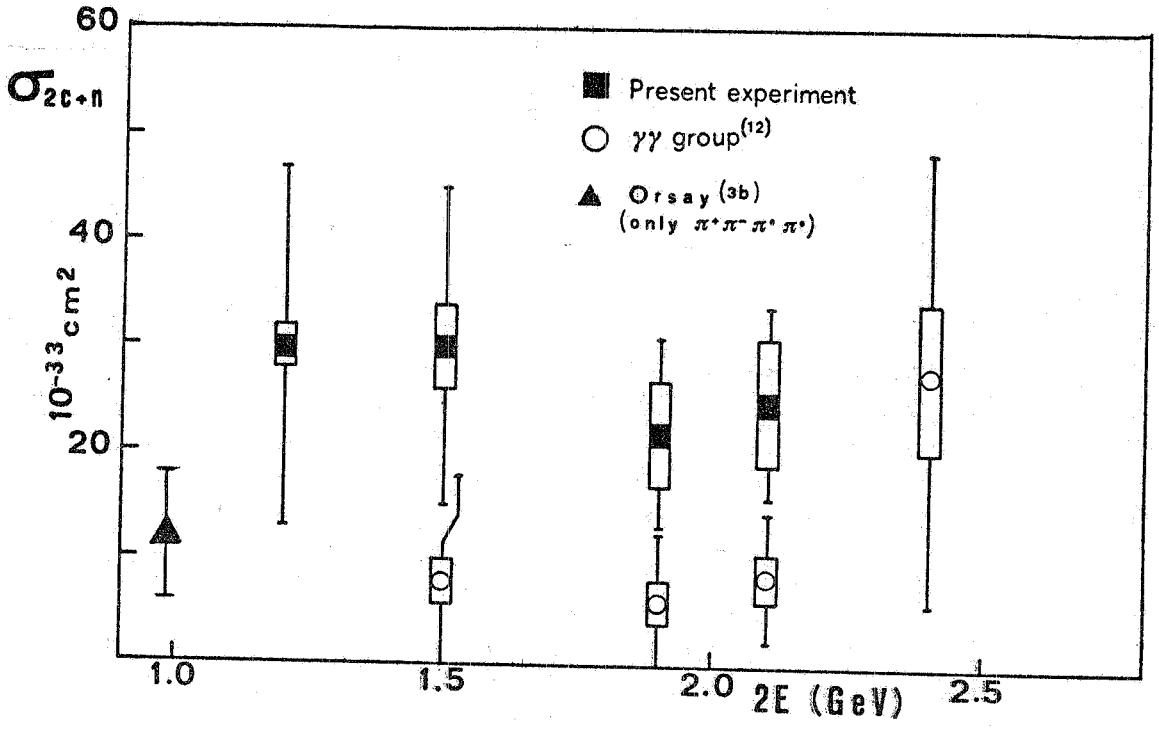

FIG. 10.1 - Energy dependence of cross section

$$\sigma_{2c+n} = \sigma(\pi^+\pi^-\pi^0) + \sigma(\pi^+\pi^-\pi^0\pi^0).$$

The open boxes indicate systematic errors. In our case these errors correspond to assuming only one of the two quoted reactions present at a time. The lower limit correspond to considering only process $e^+e^- = \pi^+\pi^-\pi^0\pi^0$.

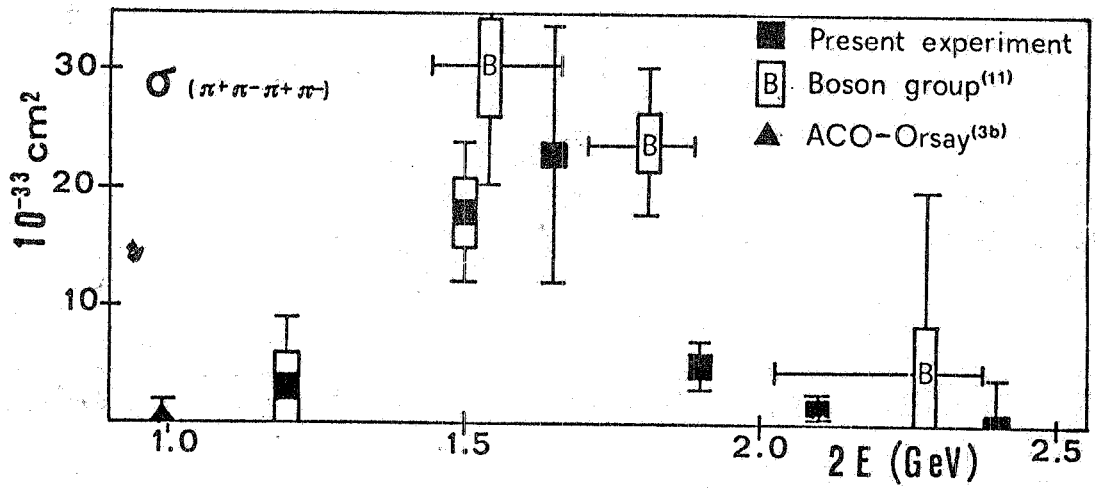

FIG. 10.2 - Energy dependence of the cross section for process $e^+e^- \rightarrow \pi^+\pi^-\pi^+\pi^-$. Also data from other groups(11)(3b) are reported for completeness. The points of the present experiment at 2E = 1, 2 and 1.5 GeV included a systematic error (see text) indicated by a open box, as in the case of the "Boson group"(11) results.

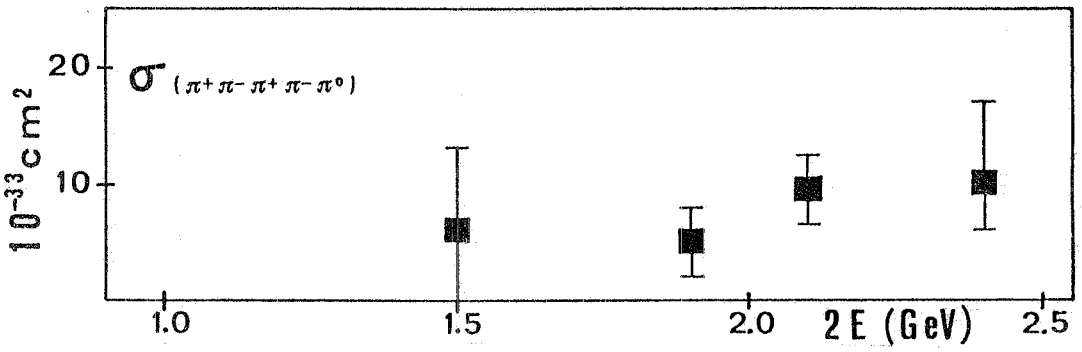

FIG. 10.3 - $\sigma(\pi^+\pi^-\pi^+\pi^-\pi^0)$ vs total energy, 2E.

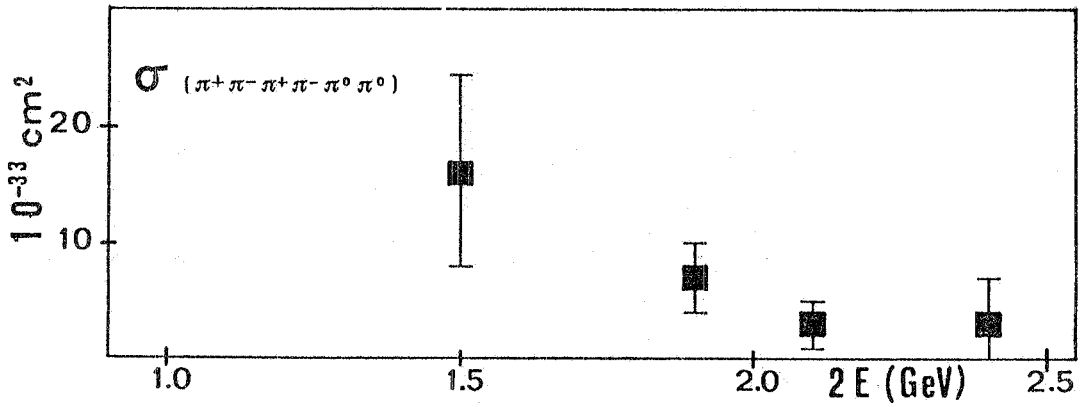

FIG. 10.4 - $\sigma(\pi^+\pi^-\pi^+\pi^-\pi^0\pi^0)$ vs total energy, 2E.

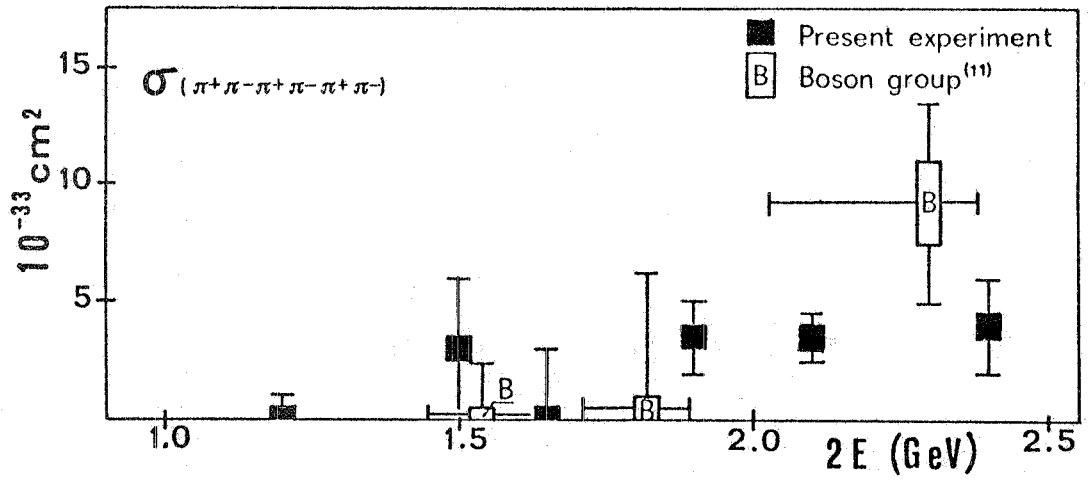

FIG. 10.6 - $\sigma(\pi^+\pi^-\pi^+\pi^-\pi^+\pi^-)$ vs total energy, 2E.

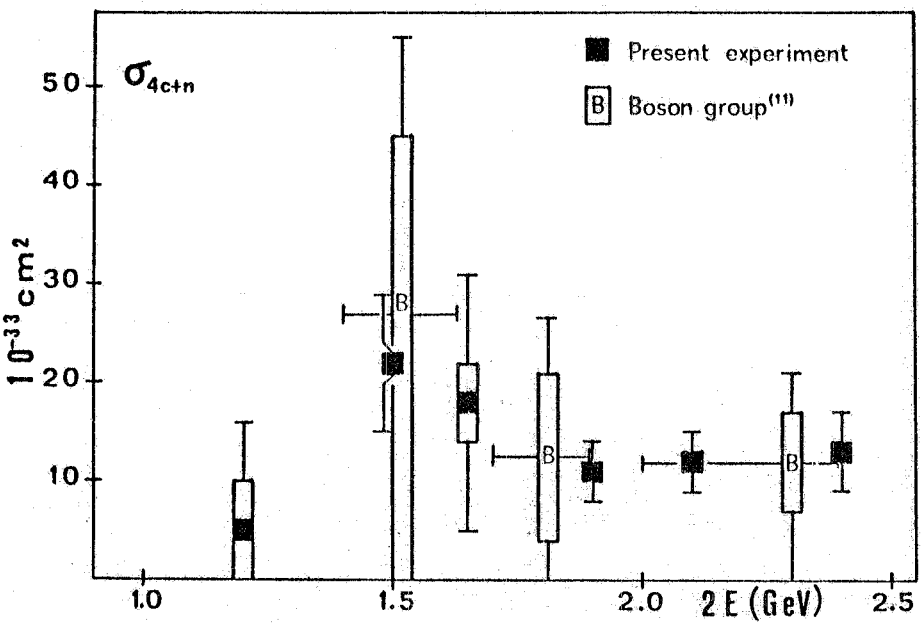

FIG. 10.5 - Energy dependence of cross section

$$\sigma_{4c+n} = \sigma(\pi^+\pi^-\pi^+\pi^-\pi^o) + \sigma(\pi^+\pi^-\pi^+\pi^-\pi^o\pi^o)$$

Also data from the "Boson group"[11] are reported for comparison. The open boxes indicate systematic errors, as in the case of Fig. 10.1.

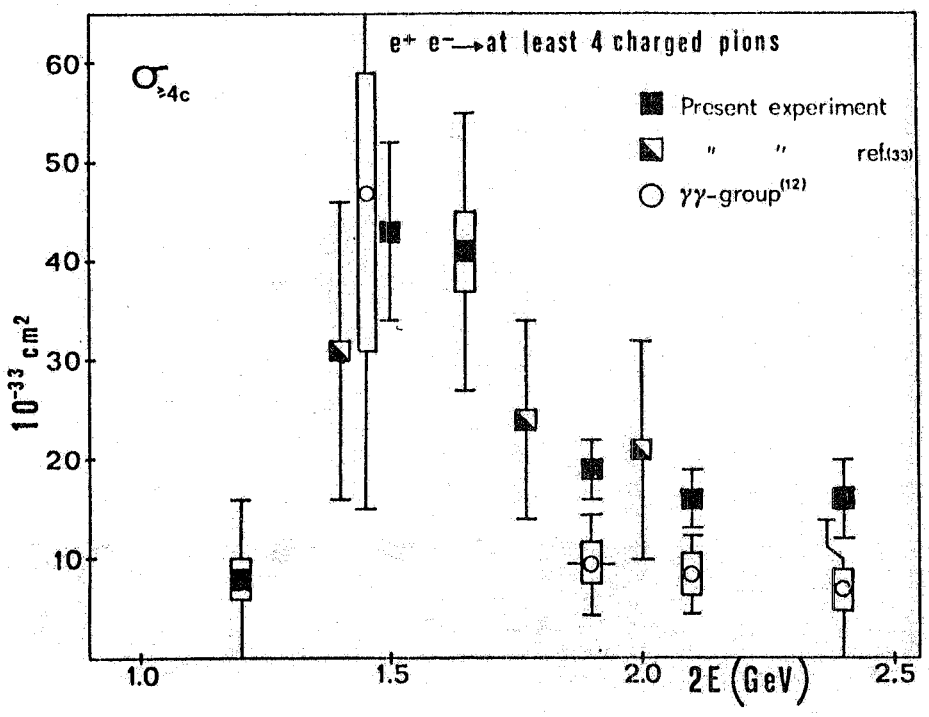

FIG. 10.7 - Energy dependence of cross section for processes in which at least four charged pions are produced, with or without neutral pions. It is assumed in our analysis that the maximum multiplicity (charged + neutrals) is six. Data from the "$\gamma\gamma$ group"[12] are also reported for comparison. Open boxes indicate systematic errors.

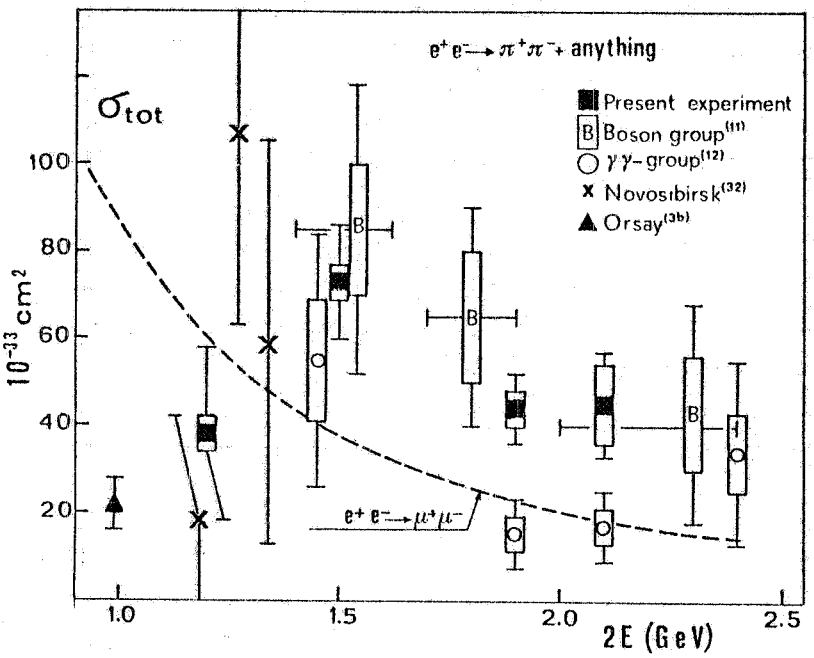

FIG. 10.8 - Energy dependence of cross section for process

$$e^+e^- = \pi^+\pi^- + \text{anything}$$

Also data from other groups working with Adone(11)(12) are shown for comparison. For completeness results from Orsay(3b) and Novosibirsk(32) are also reported. In each case open box indicate systematic errors. The dotted curve, representing the cross section for $e^+e^- \to \mu^+\mu^-$ (computed from quantum electrodinamics) is reported for reference.

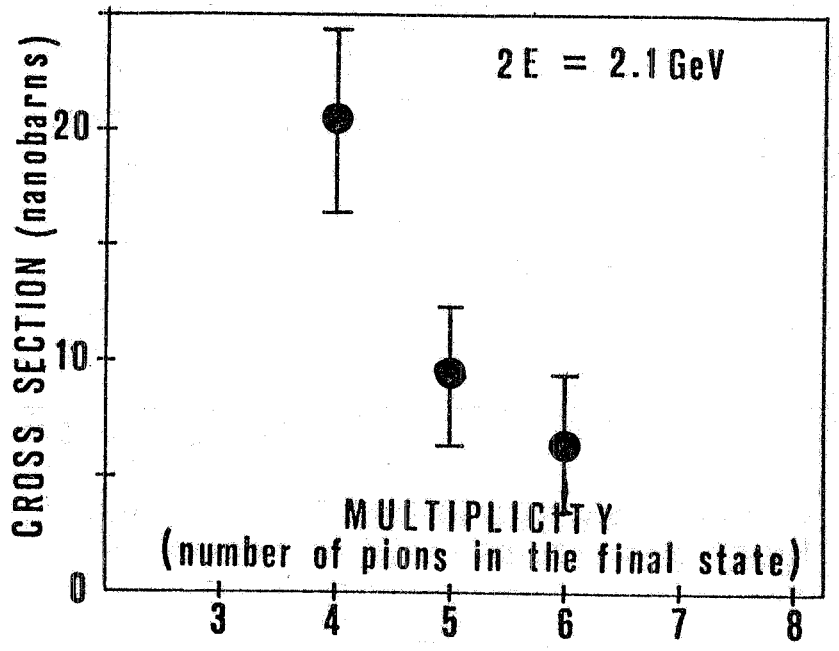

FIG. 10.9 - Total cross section for process $e^+e^- \longrightarrow \pi^+\pi^-$ + anything as function of multiplicity (i.e. total number of charged and neutral pions) at 2E = 2.1 GeV.

energy, where our results are statistically more significant and, moreover, show no indication of a resonant behaviour. The average multiplicity at 2E = 2.1 GeV results to be $\langle n_\pi \rangle \sim 4.5$. Furthermore, it does not appear to have any strong energy dependence since $\langle n_\pi \rangle$ has a value between approximately 4 and 5 over the energy range explored (2E = 1.2 ÷ 2.4 GeV).

Finally, in Fig. 10.10 we report the total cross section for final states with a positive or a negative G - parity. One can see that final states with G^+ - parity are much more abundant than those with G^- - parity, at least around 2E = 1.5 GeV.

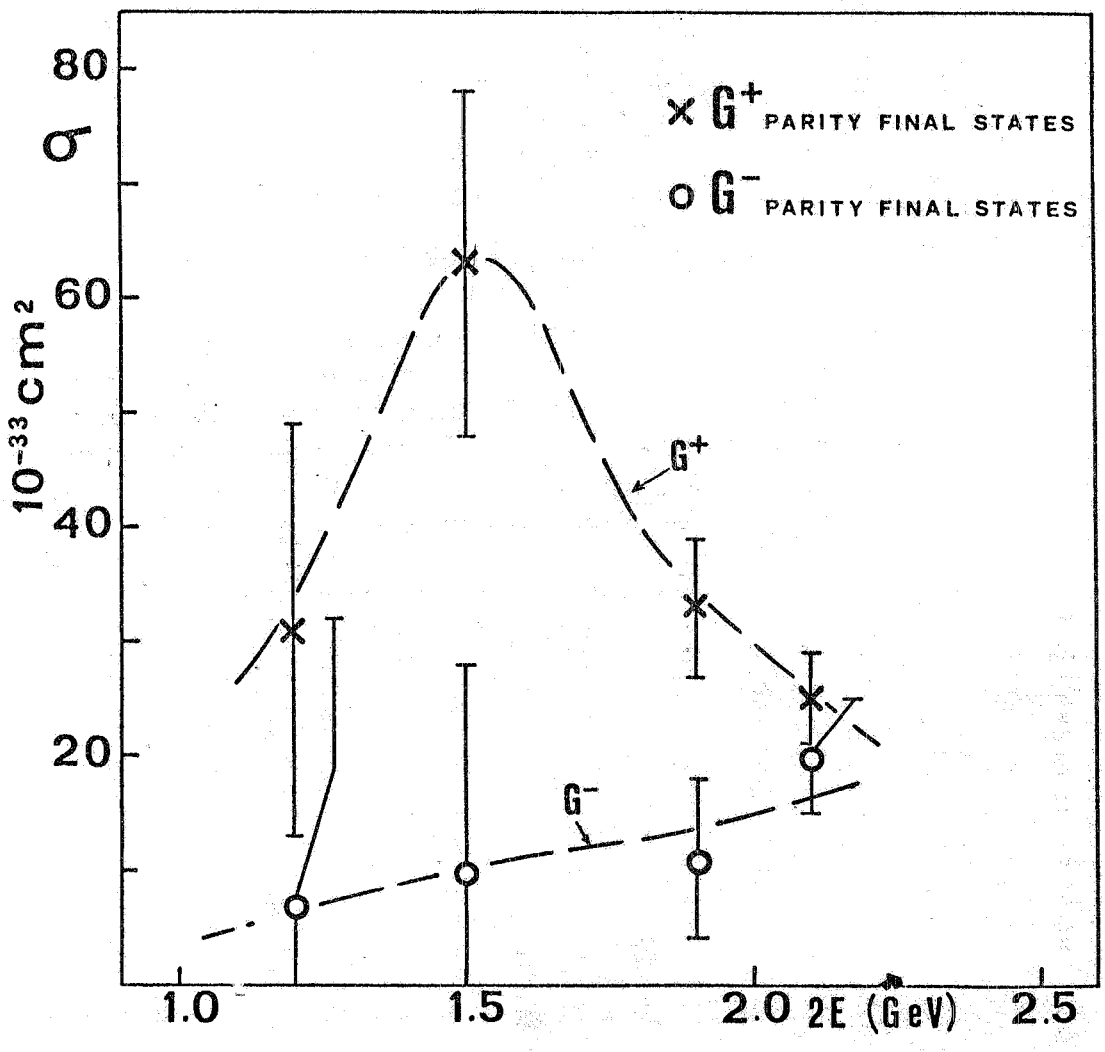

FIG. 10.10 - Cross sections relative to final states with positive and negative G-parity vs 2E.

11. - DISCUSSION AND CONCLUSIONS -

An important conclusion coming from the results reported in the previous section is that the multi-hadron production, i.e. the reaction:

(14) $$e^+e^- \longrightarrow \pi^+\pi^- + \text{anything}$$

occurs, at $2E \gtrsim 1.2$ GeV, with a total cross section, σ_{tot}, comparable to that for the annihilation process $e^+e^- \to \mu^+\mu^-$, $\sigma_{\mu\mu}$ (Fig. 10.8). The processes which contribute to reaction (14) seem to have thresholds in the neighborhood of 1 GeV. Excluding the region at low energy, where the cross section rises rapidly, the energy dependence of σ_{tot} appears to be consistent, within the large errors, with $1/E^2$; even though a less rapid energy dependence is also compatible with our results in the narrow energy interval explored. In the same energy region ($2E \gtrsim 1.5$ GeV) the ratio $\sigma_{tot}/\sigma_{\mu\mu}$ is apparently greater than 1, possible close to 2.

The total cross section, σ_{tot}, is the sum of many partial cross sections, which have been evaluated at the various energies explored. The relative weight of these cross sections depend on the total energy 2E, as one can see from the figures of the previous section. For $2E > 1.5$ GeV the contributions to σ_{tot} (Fig. 10.8) can be split into two roughly equal parts; one (σ_{2c+n}, Fig. 10.1) due to processes with only two charged pions plus neutrals; the other ($\sigma_{\geq 4}$, Fig. 10.7) due to processes with at least four charged pions in the final state. The former contribution, as mentioned already in Section 10, seems to be essentially due to the process

(5) $$e^+e^- \longrightarrow \pi^+\pi^-\pi^o\pi^o$$

On the other hand, the latter contribution comes from the following processes

(6) $$e^+e^- \longrightarrow \pi^+\pi^-\pi^+\pi^-$$

(7) $$e^+e^- \longrightarrow \pi^+\pi^-\pi^+\pi^-\pi^o$$

(9) $$e^+e^- \longrightarrow \pi^+\pi^-\pi^+\pi^-\pi^o\pi^o$$

(10) $$e^+e^- \longrightarrow \pi^+\pi^-\pi^+\pi^-\pi^+\pi^-$$

of which the first three (6), (7), (9) are responsible for the rise observed in σ_{tot} when 2E is greater than ~ 1 GeV.

Among all channels that have been studied, the one involving only four charged pions, Eq. (6), has a remarkable energy dependence,

since its cross section $\sigma(\pi^+\pi^-\pi^+\pi^-)$ exibits a broad peak at $2E \cong$ $\cong 1.6$ GeV (see Fig. 10.2). This behaviour is suggestive of the production of a vector meson, ϱ', of mass $m_{\varrho'} = \sim 1.6$ GeV/C^2, full width at half maximum $\Gamma_{\varrho'} = \sim 350$ MeV, having the same quantum numbers of the ϱ meson ($J^{PC} = 1^{--}$ and $I^G = 1^+$). Some indication in favour of the possible existence of the ϱ' meson can also be found in the results by Davier et al.[34] on the photoproduction of four pions by 6 ÷ 18 GeV γ-rays on protons. Confirming evidence comes out from a recent Berkeley - SLAC experiment[35] on four pions photoproduction in a hydrogen bubble chamber, using linearly polarized monochromatic γ rays (9.3 GeV) obtained by back scattering of a laser beam[36]. The decay angular distributions as a function of mass, derived from this last experiment, are indeed what would be expected from a ϱ' vector meson diffractively produced with helicity conservation.

An attempt can be made to evaluate the coupling constant of the presumed ϱ' meson with the photon ($g_{\varrho'\gamma} = em^2_{\varrho'}/f_{\varrho'}$), by applying the general ideas of the vector meson dominance model. Let us assume that the behaviour of $\sigma(\pi^+\pi^-\pi^+\pi^-)$, as plotted in Fig. 10.2, can be interpreted in terms of a Breit-Wigner curve. The total cross section at $2E = m_{\varrho'}$, σ^{peak}_{all}; for the process $e^+e^- \to \varrho' \to$ (all final states) is then related to the coupling costant $f^2_{\varrho'}$ by the formula:

$$\frac{f^2_{\varrho'}}{4\pi} = \frac{4\pi\alpha^2}{m_{\varrho'}\Gamma_{\varrho'}} \cdot \frac{1}{\sigma^{peak}_{all}} \tag{15}$$

where α is the fine structure constant.

Various assumptions can be made concerning σ^{peak}_{all} in order to estimate $f^2_{\varrho'}/4\pi$. We first note the following inequalities:

$$\sigma^{peak}_{all} \gtrsim \sigma^{peak}(\pi^+\pi^-\pi^+\pi^-) + \sigma^{peak}(\pi^+\pi^-\pi^0\pi^0) \tag{16}$$

and

$$\sigma^{peak}(\pi^+\pi^-\pi^+\pi^-) + \sigma^{peak}(\pi^+\pi^-\pi^0\pi^0) \gtrsim 1.25\ \sigma^{peak}(\pi^+\pi^-\pi^+\pi^-). \tag{17}$$

The first inequality is obvious, while the second is a consequence of isospin conservation in the reaction e^+e^- → four pions[37].

We can then evaluate $f^2_{\varrho'}$ in two different ways:

i) using only the data on the $\pi^+\pi^-\pi^+\pi^-$ channel, which shows resonant behaviour, and both inequalities (16) and (17) we obtain:

$$\frac{f^2_{\varrho'}}{4\pi} \lesssim 18; \tag{18}$$

ii) taking for $\sigma^{peak}(\pi^+\pi^-\pi^+\pi^-)$ and $\sigma^{peak}(\pi^+\pi^-\pi^0\pi^0)$ the

values actually measured[x] at the resonance and using the first inequality we obtain:

$$\frac{f^2_{\varsigma'}}{4\pi} \leq 10 \pm 4 \qquad (19)$$

Assuming $f^2_{\varsigma'}/4\pi \sim 10$ and taking the value of $f^2_{\varsigma}/4\pi = 2.54 \pm .23$ recently reported by Benaksas et al.[3a], one obtains for the ratio $f^2_{\varsigma'}/f^2_{\varsigma}$ a value close to 4. This agrees with the value recently predicted by Bramon and Greco[14] in their model[38] of "extended vector meson dominance", EVMD[39]. These authors[14] also predict $(\varsigma' \to \pi^+\pi^-\pi^+\pi^-)/(\varsigma' \to \pi^+\pi^-\pi^o\pi^o) \sim 1$. This is in agreement with our results, as can be seen by comparing at $2E = m_{\varsigma'} \sim 1.6$ GeV $\sigma(\pi^+\pi^-\pi^+\pi^-)$ and $\sigma(\pi^+\pi^-\pi^o\pi^o)$ (which is essentially equal to σ_{2c+n} of Fig. 10.1, as discussed in Sec. 10)[+].

It should be pointed out that direct comparison between these two cross sections cannot be made except at the ς' peak, due to possible contributions from $\varsigma\,\varsigma'$ interference. Such an interference might be responsible for the lack of a resonant behaviour in the energy dependence of the measured $\sigma(\pi^+\pi^-\pi^o\pi^o)$ (Fig. 10.1).

The hypothesis of a ς' resonance yields a simple explanation for the relatively large total cross section of multihadron production in the neighbourhood of 1.6 GeV, since the final states $\pi^+\pi^-\pi^+\pi^-$ and $\pi^+\pi^-\pi^o\pi^o$ represent $\sim 70\%$ of σ_{tot}. In this connection it is worthwhile pointing out that the hypothesis of a ς' resonance, with positive G-parity (G^+), is also supported by the results displayed in Fig. 10.10, where, around 1.6 GeV, final states with G^+-parity are seen to be much more abundant than final states with G^--parity[o].

(x) - In inserting the numerical values of the measured cross sections in Eq. 16 there is an implicit assumption made that the non-resonant background is not greater than the neglected resonant contributions. Such an assumption is in line with what is expected from the model discussed in ref. (14) and the ς tail contribution to the two quoted four pion channels, computed in ref. (41 d).

(+) - In drawing any conclusion on this matter, a word of caution is needed, however, since the $\pi^+\pi^-\pi^o\pi^o$ channel is even less well established experimentally than the channel $\pi^+\pi^-\pi^+\pi^-$. The γ-γ group at Adone, as mentioned earlier, find a somewhat lower values for $\sigma(\pi^+\pi^-\pi^o\pi^o)$ than ours.

(o) - See footnote at pag. 48.

New models of EVMD recently proposed[39] claim the existence of other resonances besides the ϱ' (ω' and ϕ', e.g., as SU_3 partners of ϱ'; and possibly further SU_3 nonet). These higher resonances might be responsible for the large values of σ_{tot} observed at the largest energies attained in our experiment(x). Further measurements are needed, of course, to establish whether these new resonances, including the ϱ', do really exist. Should this be the case, the physics of e^+e^- colliding beams in the GeV region would be clearly characterized by these new resonances. On the other hand, if new resonances are not present there remains the problem of explaining a cross section which is possibly a factor 2 larger than the cross section for $e^+e^- \rightarrow \mu^+\mu^-$. A possible explanation can be searched in terms of the well known SLAC results on deep-inelastic electron-nucleon scattering, where the discovery of a scale-invariant behaviour[42] is very suggestive of a parton structure of the nucleon[43]. As suggested by various authors[44], the connection between colliding beams and deep inelastic results, and, therefore, significant information on the hadron structure, could be obtained by measuring in e^+e^- collisions in the asymptotic region the following:

i) the energy dependence of the total cross section for hadron production, σ_{tot};

ii) the ratio $\sigma_{tot}/\sigma_{\mu\mu}$;

iii) the energy dependence of hadron multiplicity[45].

As an example let us considerer point (ii), where different theoretical approaches, based on the general concepts of the light cone and of the quark models have been developed(+). Using the approach based on fundamental <u>free</u> spin 1/2 quark fields[46], one obtains $\sigma_{tot}/\sigma_{\mu\mu} = 2/3$.

(o) - The separation into final states of opposite G-parity turns out to be useful also for one of the possible comparisons between e^+e^- data at $2E \sim 2$ GeV and data from nucleon-antinucleon annihilation. Recently a specific model has been proposed[40] for such a connection, but unfortunately it predicts a ratio G^+ over G^--states as large as ~ 35; much larger than the one observed (Fig. 10.10).

(x) - Attempts have also been made[41] to interpret the multihadron production observed with Adone within the framework of the "classic" vector meson dominance model. They do not seem capable, however, of explaining the experimental situation, without introducing very specific and somewhat questionable assumptions.

(+) - A recent discussion on quark model predictions can be found in H. Suura, T.F. Walsh and Bing-LinYoung: Desy report 72/21 (May 1972).

Different values for this ratio are obtained if one introduces elementary particles constituents, or partons, of spin 0[49]. The new quark model recently proposed by Gell-Mann[47], predicts $\sigma_{tot}/\sigma_{\mu\mu} = 2$; a value which is also predicted by Han and Nambu on the basis of a different quark model[48]. On the other hand, the EVMD model of Bramon, Etim and Greco quoted above[39] predicts $\sigma_{tot}/\sigma_{\mu\mu} \sim 1.25$. Unfortunately, at the present stage of this research, the results concerning the absolute value and energy dependence of σ_{tot}, as well as the energy dependence of the average multiplicity, cannot discriminate between the different theoretical predictions. This is not only because of the large uncertainties in the measured quantities, but also because there are at present no reasons to believe that the asymptotic region is already reached at Adone energies.(x)

In closing the present discussion, we wish to recall that all cross sections have been calculated assuming invariant phase space only(+). As an indication of the insensitivity of the results to this assumption we have recalculated the cross section for the process (6) under a quite different hypothesis. Assuming, as an example, that the final state $(\pi^+\pi^-\pi^+\pi^-)$ is reached through the intermediate quasi-two-body virtual state $A_1\pi$, $(e^+e^- \to A_1^{\pm}\pi^{\mp} \to \pi^+\pi^+\pi^-\pi^-)$, we find a cross section which, at all energies, does not exceed that obtained assuming invariant phase space by more than 20%. So we feel that the assumption of invariant phase space adopted throughout our analysis, should not affect the general conclusions reached in the previous discussion.

The principal results of this experiment may be summarized as follows:

1) Multi-hadron production by e^+e^- beams colliding at GeV energies, occurs with a total cross section, σ_{tot}, comparable to that of the annihilation process $e^+e^- \to \mu^+\mu^-$, $\sigma_{\mu\mu}$, (see Fig. 10.8). In particular at the highest energies attained ($2 \div 2.4$ GeV), $\sigma_{tot}/\sigma_{\mu\mu}$ is apparently greater than 1, possible close to 2.

2) The energy dependence of σ_{tot} exibits a fast rise near 1 GeV. For $2E \gtrsim 1.5$ GeV the energy dependence of σ_{tot} is compatible with $1/s$ ($s = 4E^2$).

(x) - If this were the case, the observed energy dependence of the average multiplicity (Sec. 10) would not be in agreement with the predictions of the particularly simple statistical model proposed by Bjorken and Brodsky[45d], i.e. $\langle n_\pi \rangle \propto E$.

(+) - An exception is the cross section $\sigma(\pi^+\pi^-\pi^0\pi^0)$ measured at ACO[3b], where the value was derived assuming the specific process $e^+e^- \to \omega\,^0\pi^0 \to \pi^+\pi^-\pi^0\pi^0$. This value is given in Fig. 10.1.

3) The average multiplicity (charged plus neutral pions) is found to be between 4 and 5, over the energy range explored. At 2E = 2.1 GeV, above the ς' region, the average multiplicity $\langle n_\pi \rangle \cong 4.5$ (See Fig. 10.9).

4) Final states with positive G-parity (G^+) are found to be much more abundant than G^- final states (see Fig. 10.10).

5) G^+ final states are made up mostly of four pions ($\pi^+\pi^-\pi^o\pi^o$ and $\pi^+\pi^-\pi^+\pi^-$), with $\sigma(\pi^+\pi^-\pi^o\pi^o) + \sigma(\pi^+\pi^-\pi^+\pi^-) \cong 0.7\ \sigma_{tot}$.

6) The energy dependence of $\sigma(\pi^+\pi^-\pi^+\pi^-)$ is suggestive of a resonance behaviour (see Fig. 10.2). This may be interpreted in terms of a ς' meson of mass $m_{\varsigma'} \sim 1.6$ GeV/c^2 and $\Gamma_{\varsigma'} \sim 350$ MeV, coupled to the photon with a coupling constant $(g_{\gamma\varsigma'} = em^2/f^2_{\varsigma'})\ f^2_{\varsigma'}/4\pi \leq$ ≤ 18.

7) The existence of the ς' meson would yield a straightforward explanation for the large cross section around 1.6 GeV. At higher energies other resonance should be invoked, in a resonant model, to explain the relatively large cross section observed up to the higher total energy attained in this experiment.

ACKNOWLEDGMENTS -

The present experiment was made possible by the active cooperation of the accelerator group at Adone under the leadership of Prof. F. Amman. Particular thanks are due to Dr. M. Placidi for his continuous efforts in keeping the machine operation as efficient as possible.

We wish to express warmly our gratitude to Prof. G. Barbiellini who greatly contributed to the first stage of the experiment. Thanks are also due to Dr. G. Barbarino and G. Giannoli for their partecipation in the analysis of the events and to M. Bertino, G. Nicoletti and A. Pecchi for their invaluable help in solving many technical problems during the preparation and running of the experiment. We thank our scanners, particularly E. Cecarelli, for their collaboration during the scanning and the analysis of the events. The important contribution made by the machinery shops in Rome and at Frascati, under the guidance of Mr. A. Pellizzoni and Mr. G. Di Stefano, respectively, is gratefully acknowledged.

We thank Professors N. Cabibbo, S. D. Drell and R. Gatto for illuminating discussions on some of the more fundamental theoretical aspects underlying this research.

Finally, special thanks are due to Drs. A. Bramon and M. Greco for their continuous interest and for many valuable conversations which helped to clarify the interpretation of our experimental results.

APPENDIX A -

A more complete and detailed description of the apparatus[50] is given in this Appendix. The dimensions of the counters and the kinematic spark chamber C1, that limit the solid angle, are listed in table A1. A complete list of dimensions of the absorbers and all active elements is given in table A2 (see also Fig. 2.1).

TABLE A1

Counters and spark chamber limiting the solid angle

Element	a (cm)	b (cm)	d (cm)
Counter 0	$\pm$ 30	$\pm$ 13.5	14
Spark Chamber C_1	$\pm$ 37	$\pm$ 30	24
Counter 1	$\pm$ 36.5	$\pm$ 30	30
Counter 2	$\pm$ 40	$\pm$ 40	45
Counter 3	$\pm$ 50	$\pm$ 50	64
Counter 4	$\pm$ 60	$\pm$ 60	82

a = horizontal half width
b = vertical half height
d = distance from center of the straight section.

It must be mentioned that heavy shielding of concrete and lead ($\sim$ 40 r.l.) has been placed around the telescopes in the horizontal plane, where the beam losses are mostly confined. To obtain a further reduction of the trigger rate due to machine background, it was also necessary to have 1 radiation length of lead before counters I_1, E_1 and the same amount in front of counters I_2, E_2. This last material was actually made up of two water Cerenkov counters C_I, C_E. These counters were not used in the trigger, but their outputs were displayed in the "DATA Box" (see Sec. 2 and Fig. A1) to be used in the analysis. They were effective in selecting K meson pairs from $\pi\pi$ pairs, because the K meson velocity is below the threshold for Cerenkov light for A-done energies up to 2E = 1.5 GeV.

The presence in the trigger of counters 0, always was required in various combinations, and they helped especially in reducing cosmic ray background for collinear muons[28].

In fact each set of counters I_o and E_o consists of three horizontal slab of scintillators, each one with their photomultiplier so that, with the appropriate electronic logic described below, in the case of selection of muon pair, it was possible to narrow down the bounds of the central region surrounding the actual source. All counters, except I_o, E_o, I_1,

TABLE A2 - Thickness of elements of the telescope

	material	mm	g/cm^2 (Fe eq.)	rad. lenght	Inter. lenght
Vacuum Chamber: Window	Fe	.2	.2	.01	.001
Body	Fe	6	4.7		
Counter 0	CH	10	1.5	.02	.015
Spark Chamber C_1	Al	1.8	.5	.02	.006
Absorber	Pb	5	4.3	.98	.032
Counter 1	CH	10	1.5	.02	.015
Absorber	Pb	5	4.3	.98	.032
Cerenkov Counter C	Al	10	3.0	.11	.029
	CH	10	1.5	.02	.015
	H_2O	60	8.8	.17	.074
Counter 2	CH	20	3.0	.05	.030
Spark Chamber C_2	Fe	19.5	15.2	1.13	.128
Counter 3	CH	20	3.0	.05	.030
Spark Chamber C_3	Fe	34	26.5	1.95	.224
	Al	32	10.0	.36	.094
Counter 4	CH	20	3.0	.05	.030
Absorber ($\frac{1}{2}$ of $\Delta\Omega$)	Fe	140	110	8.0	.92
Absorber	Fe	90	70	5.15	.59
Absorber (shaped)	Fe	140 (max)	110	8.0	.92
Counter 5	CH	20	3.0	.05	.030
Spark Chamber C_4 (only one)	Al	15	4.5	.16	.043
	Fe	37.5	33.7	2.31	.29

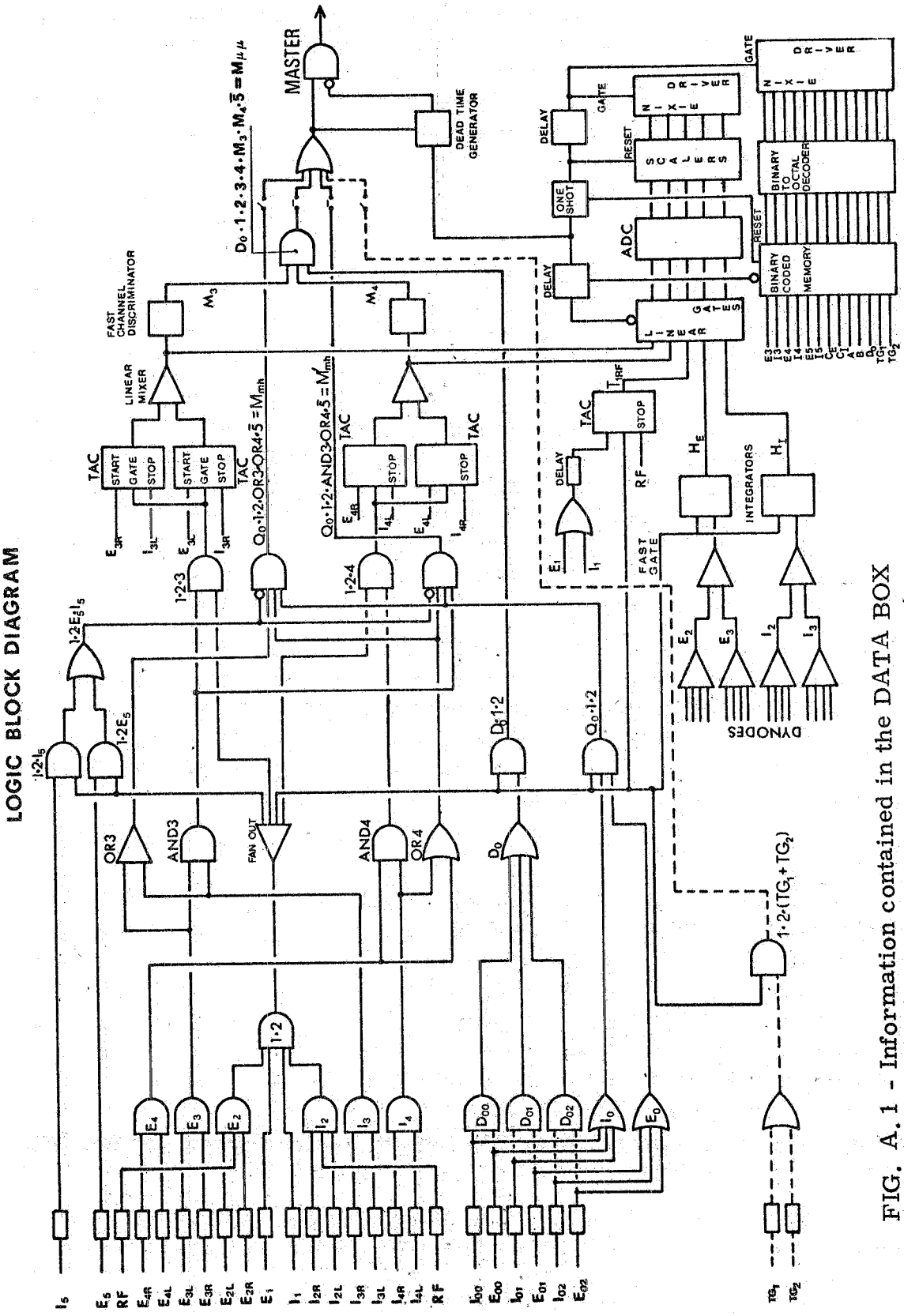

FIG. A. 1 - Information contained in the DATA BOX photographed in addition to the two views of the spark chambers.

E_1, had phototubes placed on apposite edges of the scintillator (e.g. I_{2R}, I_{2L}, E_{2R}, E_{2L}, etc.) and they were put in coincidences between themselves before entering into the rest of logic circuits. By this arrangement, the efficiency for detecting charged particles in the light pipes was pratically reduced to zero, while the overall efficiency of the scintillator was always $\sim$ 99%. Such improvement was very helpful, not only to reduce background, but especially to define the active region of the counter itself.

Counters E_3, I_3, E_4, I_4 were employed also to measure the time delay between the opposite pairs, as explained in Sec. 2, and in this case the output pulses from the two side of the scintillator were used individually in order to minimize the effect of the large dimensions of these counter[24].

This time information was elaborated by fast circuits, in order to be used in the formation of the master trigger. Its description follows (see block diagram fig. A2). The opposite sides of counters I_3, E_3 and I_4, E_4 (e.g. I_{3L}, E_{3R}) were fed to four time to amplitude converters (TAC), acting as START and STOP pulses; the gate pulse was provided in each case by the suitable coincidence (i.e. E1•I1•E2•I2•E3•I3) for the timing between the counters 3 and similarly for counters 4.

The outputs of the two time-to-amplitude converters for each opposite pair of counters was linearly mixed and fed to a fast window discriminator. Thus the simultaneous crossing of the counters by collinear particles produced in e^+e^- collision, gave a pulse, the average amplitude of which was in the middle of the limits imposed by the single channel discriminator. The same pulse, without any shaping, was also converted in digital form and displayed on the DATA BOX for further analysis (see fig. 6.1).

Since cosmic rays cross the counters of each pair with a time delay equal to their distance divided by the speed of light ($\sim$9 nsec for counters 3 and $\sim$ 12 ns for counters 4), they will produce in the time of flight spectrum two peaks, in the valley between them being located the "good events". This method, as explained in Sec. 2, cannot be employed in selecting other processes than μ pair annihilation since it requires particles penetrating until counters 4 on both telescope. Therefore an alternative trigger employed the veto signal provided by any of the counters E_5, I_5, located in the upper half of the apparatus. The reduction factor in this case was of $\sim$ 1/40.

A third method, common to both triggers, was used to reduce the contribution given by cosmic rays. A fast coincidence was formed with the phase signal of the accelerating radiofrequency RF and the counters E_1, I_1. The resolution in the prompt coincidence was of 20 ns. To improve the discriminating power of this device, it was used a time to amplitude converter (TAC), the START of which was given by the mixed signals from counters E_1, I_1 and the STOP was provided again by the RF. The

DAY	MONTH	HOUR	MIN

no bunch

Pattern	Luminosity
H_E	T_{33}
H_I	T_{44}
T_{1RF}	Photogramme N.

Pattern: (coded in octal number)

1st digit: bit 0: $M_{\mu\mu}$
1: M_{mh}
2: D_o

2nd 0: E_3
1: I_3
2: E_4

3rd 0: I_4
1: E_5
2: I_5

4th 0: $\check{C}_E$
1: $\check{C}_I$
2: A

5th 0: B

"DATA BOX"

FIG. A.2 - Logic block diagram of fast electrohics employed in the experiment.

analog output was digitized and displayed on the DATA BOX. The ultimate resolution (see fig. 3.1) was then 4 ns (FWHM), due essentially to the dimensions of counters 1, since the time overlap between the two e^+e^- bunches is about 2 ns.

Finally, the different kind of triggers, formed using alternative logics, were logically mixed in a OR circuit to produce the Master trigger to all apparatus. The two sets of triggers were:

(A1) $$M_{\mu\mu} = D_o \cdot 1 \cdot 2 \cdot 3 \cdot 4 \cdot M_3 \cdot M_4 \cdot RF$$

(A2) $$M_{mh} = Q_o \cdot 1 \cdot 2 \cdot (E_3+I_3) \cdot (E_4+I_4)\overline{(E_5+I_5)} \cdot RF$$

where

- 1, ..., 4 stand for twofold coincidences $E_1 \cdot I_1$, ..., $E_4 \cdot I_4$.
- D_o stands for the "OR" of the three coincidences formed by pairs of 0 counters opposite to respect to the source line (i.e. $D_o = (I_{oo} \cdot E_{o2}) + (I_{o1} \cdot E_{o1}) + (I_{o2} \cdot E_{oo})$)
- Q_o stands for the two fold coincidence btween any opposite pair of counters 0 (i.e. $Q_o = (E_{oo}+E_{o1}+E_{o2}) \cdot (I_{oo}+I_{o1}+I_{o2})$)
- $M_3(M_4)$ stands for the result of the fast elaboration of time delay between counters 3 (4).

Because of the machine background at higher energies, the trigger (A2) was modified in order to maintain the rate to about 1/min. At machine energies greater than 2E = 2 GeV the trigger (A2) was then replaced by:

(A3) $$M'_{mh} = Q_o \cdot 1 \cdot 2 \cdot 3 \cdot (E_4+I_4) \cdot \overline{(E_5+I_5)} \cdot RF$$

Instead, at machine energies lower than 2E = 1,5 GeV, it was possible to reduce the energy threshold for a particle in order to produce a trigger, by avoiding the request of counters 4. This fact was especially important for K meson, since their range was less than the amount of material before counter 4. The trigger replacing trigger (A2) was then:

(A4) $$M''_{mh} = Q_o \cdot 1 \cdot 2 \cdot (E_3+I_3) \cdot \overline{(E_5+I_5)} \cdot RF$$

Of course, in the computation of integrated cross sections and efficiencies, any variation in the trigger mode was accounted for. Electron pairs were able to produce both kind of triggers $M_{\mu\mu}$ and M_{mh}, thus providing a very convenient mean of testing the performance of the apparatus by cross checks, in most cases, of the efficiencies of individual counters.

The Master trigger was acting the general gate to open the linear integrators giving the charges collected during 80 ns from E_2+E_3 (H_E) and from I_2+I_3 (H_I). The analog output was displayed on the DATA BOX

and a second output was used with a multichannel pulse height analyzer to perform occasional tests during data taking and with cosmic rays. The same utility was provided for the analog output T_{33}, T_{44} and T_{1RF}, so that the stability of all apparatus was under constant control.

A parallel input register (BINARY CODED MEMORY in the block diagram), capable of storing the fast pulses coming from individual counters (see Sec. 2), was opened at the occurrence of a Master trigger, its binary content was coded in octal form and displayed on the "DATA BOX".

Most of the electronic equipment was installed in the machine hall, at a distance of a few meters from the center of the straight section. During Adone operation, however, no access was permitted over this region, for reasons of radiation safety. Hence, all checks of the correct operation of the apparatus and related electronics had to be made in the control-hall provided for this purpose, at a distance of some 20 meters. The triggering conditions of the electronics installed in the machine hall could be changed by remote-switching operation, so as to allow one to realize promptly the triggering conditions appropriate for specific tests (for example, cosmic rays measurements).

All the relevant information contained in the DATA BOX, was also reproduced in the control-hall by means of nixie-lamps, which repeated the same numbers appearing in the photograph. A set of scalers giving numbers of events, time interval, and additional useful information was also installed in the control-hall. The content of these scalers was authomatically printed on paper at regular intervals of 20 minutes.

The HT of the phototube power supplies was automatically reduced to about 1.2 KV whenever the magnetic field of Adone was below a fixed value depending on the machine energy. Therefore during the injection of electrons or positrons in the ring, no damage would result from very intense bursts of particles on the photomultipliers.

On account of the authomatic controls mentioned above, no continuous presence of physicists or operators was required during the ordinary runs.

The optical system used to bring the two orthogonal views of the apparatus onto the same photographic camera, consisted of a set of plane mirrors placed at $\sim 45^{\circ}$, some of which of very unusual length ($\sim$ 4 m). A single picture frame of 70 mm x 100 mm (Sec. 2), contained the two stereoviews with all the information given in digital form by the DATA BOX. The demagnification factos was 1/50. The camera, located at 18 m from the center of the apparatus, was usually loaded with a Ferrania P30 film roll of 120 m, lasting on the average about 10 hours.

REFERENCES -

(1) - For a comprehensive discussion on the physics of high energy e^+e^- colliding beams we refer the reader to a well-known paper by N. Cabibbo and R. Gatto: Phys. Rev. 124, 1577 (1961).

(2) - V.E. Balakin, G.I. Budker, E.V. Pakhtusova, V.A. Sidorov, A.N. Skrinskij, G.M. Tumaikin, A.G. Khabakhprashev, Phys. Lett. 34 B, 328 (1971).

(3) - See, also for previous reference:
(a) D. Benaksas, G. Cosme, B. Jean-Marie, S. Jullian, F. Laplance, J. Lefrançois, A.D. Liberman, G. Parrour, J.P. Repellin and G. Sauvage, Phys. Lett. 39 B, 289 (1972).
(b) J. Lefrançois, Proceedings of the International Symposium on Electron and Photon Interactions at High Energies, (Cornell University,Ithaca N.Y., 1971), pag. 51.

(4) - See for instance:
(a) W.K.H. Panofsky, Comments on Nuclear and Particle Physics 4, No. 5 (1970).
(b) J.J. Sakurai, Invited paper at Balaton Symposium on Hadron Spectroscopy (Sept. 1970), in Acta Physica Hungarica 31, (1-3) pag. 5 (1972).
(c) S.D. Drell, Rapporteur talk at the International Conference on Elementary Particles, Amsterdam, 1971.
(d) J.D. Bjorken, Rapporteur talk at the International Symposium on Electron and Photon Interactions at High Energies, Cornell (August-Sept. 1971).

(5) - F. Amman, R. Andreani, M. Bassetti, M. Bernardini, A. Cattoni, V. Chimenti, G.F. Corazza, D. Fabiani, E. Ferlenghi, A. Massarotti, C. Pellegrini, M. Placidi, M. Puglisi, F. Soso, S. Tazzari, F. Tazzioli and G. Vignola, Lettere Nuovo Cimento 1, 729 (1969).

(6) - (a) B. Borgia, M. Conversi, M. Grilli, E. Iarocci, M. Nigro, L. Paoluzi, P. Spillantini, L. Trasatti, V. Valente, R. Visentin and G.T. Zorn, Frascati LNF 71/62 (1971); presented at the Intern. Symposium on Electron and Photon Interactions at High Energies Cornell (Sept. 1971).
(b) V. Alles-Borelli, M. Bernardini, D. Bollini, T. Massam, L. Monari, F. Palmonari, A. Zichichi, Invited paper (Presented by A. Zichichi) in the Proceedings of the International Conference of E.P.S. on Meson Resonances and Related Electromagnetic Phenomena (Bologna, 1971).

(7) - (a) V. Alles-Borelli, M. Bernardini, D. Bollini, P.L. Brusini, E. Fiorentino, T. Massam, L. Monari, F. Palmonari, F. Rimondi and A. Zichichi, Cern Preprint, Geneve, May 1972.
(b) G. Barbarino, F. Ceradini, M. Conversi, S.D'Angelo, E. Iarocci, M. Grilli, M. Nigro, L. Paoluzi, R. Santonico, P. Spillantini, L. Trasatti, V. Valente, R. Visentin and G.T. Zorn (in progress).

(8) - (a) G. Barbiellini, M. Conversi, M. Grilli, A. Mulachié, M. Nigro, L. Paoluzi, P. Spillantini, R. Visentin and G.T. Zorn, Frascati LNF-70/38 (1970), Proceedings of the 15th International Conference on High Energy Physics,Kiev, 1970, pag. 704.
(b) B. Bartoli, B. Coluzzi, F. Felicetti, G. Goggi, G. Marini, F. Massa, D. Scannicchio, V. Silvestrini and F. Vanoli, Nuovo Cimento 70 A, 615 (1970).
(c) V.E. Balakin, G.I. Budker, I.B. Vasserman, O.S. Koitman, L.M. Kurdadge, S.I. Mishnev, A.P. Omuchin, S.I. Seredryakov, V.A. Sidorov, A.N. Skrinsky, G.M. Tumaikin, V.F. Turkin, A. G. Khabakhpashev and J.M. Shatunov, Novosibirsk Internal Report 62/70 (1970); Proceedings of the 15th International Conference on High Energy Physics (Kiev, 1970), pag. 705.
(d) R. Wilson, Proceedings of the 15th International Conference on High Energy Physics, Kiev (August-Sept. 1970), pag. 219.

(9) - (a) "$\mu\pi$ group": invited talk (presented by M. Conversi) in the Proceedings of the International Conference of E.P.S. on Meson Resonances and Related Electromagnetic Phenomena (Bologna, 1971).
(b) "$\gamma\gamma$ group": invited talk (presented by G. Salvini) in the Proceedings of the International Conference of E.P.S. on Meson Resonances and Related Electromagnetic Phenomena (Bologna, 1971).

(10) - B. Bartoli, F. Felicetti, G. Marini, A. Nigro, H. Ogren, N. Spinelli, V. Silvestrini and F. Vanoli, Phys. Letters 36 B, 598 (1971).

(11) - B. Bartoli, F. Felicetti, G. Marini, A. Nigro, H. Ogren, V. Silvestrini and F. Vanoli, Frascati LNF-71/91 (submitted to the Physical Review).

(12) - C. Bacci, R. Baldini-Celio, G. Capon, C. Mencuccini, G.P. Murtas, G. Penso, A. Reale, G. Salvini, M. Spinetti and B. Stella, Physics Lett. 38 B, 551 (1972).

(13) - G. Barbarino, F. Ceradini, M. Conversi, M. Grilli, E. Iarocci, M. Nigro, L. Paoluzi, R. Santonico, P. Spillantini, L. Trasatti, V. Valente, R. Visentin and G.T. Zorn, Lett. Nuovo Cimento 3, 689 (1972).

(14) - A. Bramon, M. Greco, Lett. Nuovo Cimento 3, 693 (1972).

(15) - B. Borgia, F. Ceradini, M. Conversi, M. Grilli, A. Mulachié, L. Paoluzi, W. Scandale, P. Spillantini and R. Visentin, Phys. Lett. 35 B, 340 (1971).

(16) - "Gruppo Adone" Frascati LNF - 70/48 (1970); Frascati LNF-71/7 (1971), presented at the 1971 National Particle Accelerator Conference, Chicago.

(17) - V. Alles-Borelli, M. Bernardini, D. Bollini, P.L. Brunini, E. Fiorentino, T. Massam, L. Monari, F. Palmonari and A. Zichichi, Nuovo Cimento 7 A, 345 (1972).

(18) - G. Barbiellini, B. Borgia, M. Conversi and R. Santonico: Atti

Acc. Naz. Lincei 44, 233 (1968).
(19) - G. Barbiellini, S. Orito - Frascati LNF-71/17 (1971).
(20) - See, also for previous references of theoretical papers on the same subject: S.J. Broodsky, T. Kinoshita and H. Terazawa, Physics Rev. 4D, 1532 (1971).
(21) - V.E. Balakin, A.D. Bukin, E.V. Pakhtusova, V.A. Sidorov, and A.G. Khabakhpaskev, Phys. Lett. 34 B, 663 (1971).
(22) - C. Bacci, R. Baldini-Celio, G. Capon, C. Mencuccini, G.P. Murtas, G. Penso, A. Reale, G. Salvini, M. Spinetti and B. Stella, Lett. Nuovo Cimento 3, 709 (1972).
(23) - B. Borgia, F. Ceradini, M. Conversi, L. Paoluzi, R. Santonico, G. Barbiellini, M. Grilli, P. Spillantini, R. Visentin and F. Grianti, Lett. Nuovo Cimento 3, 115 (1972).
(24) - L. Paoluzi and R. Visentin, Nucl. Instr. and Meth. 65, 345 (1968); B. D'Ettorre-Piazzoli and R. Visentin, Frascati LNF-69/65 (1969).
(25) - A summary of these data can be found in H. Ogren, Frascati LNF-71/89 (1971).
(26) - J.E. Augustin, P. Marin and F. Rumpf, Nucl. Instr. and Meth. 36, 213 (1965).
(27) - C. Baltay, P. Franzini, G. Lütjens, J.C. Severtens, D. Tycho and D. Zanello, Phys. Rev. 145, 1103 (1966).
(28) - See, for instance: E. Lillethun, Proceedings of the International Conference on Elementary Particles, Lund (1969), pag. 165; M. G. Albrow, D.P. Barber, A. Bogaerts, B. Bosnjakovic, J.R. Brooks, A.B. Clegg, F.C. Ernè, C.N.P. Gee, A.D. Kanaris, A. Lacourt, D.H. Locke, P.G. Murphy, A. Rudge, J.C. Sens and F. van der Veen, Phys. Letters 40 B, 136 (1972).
(29) - R. Kajikawa, Journal of Phys. Soc. 18, 1365 (1963); H. Thom, Phys. Rev. 136, B 447 (1964); Z.S. Strugalski, JINR Dubna report E 13-5152 (1970);
(30) - G. Barbarino, F. Ceradini, M. Conversi, S. D'Angelo, K. Ekstrand, E. Iarocci, M. Grilli, M. Nigro, L. Paoluzi, R. Santonico, P. Spillantini, L. Trasatti, V. Valente, R. Visentin and G. T. Zorn, (in progress).
(31) - G. Barbarino, F. Ceradini, M. Grilli, E. Iarocci, M. Nigro, L. Paoluzi, R. Santonico, P. Spillantini, L. Trasatti, V. Valente, R. Visentin, G.T. Zorn, Frascati-LNF-72/42 (1972).
(32) - V.E. Balakin, G.I. Budker, I.B. Vasserman, O.S. Koifman, L. M. Kurdadze, S.I. Mishrrev, A.P. Onuchin, S.I. Serednyakov, V.A. Sidorov, A.N. Skrinsky, G.M. Tumaikin, V.F. Tusckin, A.G. Khabakpashev, J.M. Shatunov in V.A. Sidorov, Proceedings of the International Symposium on Electron and Photon Interactions at High Energy - Cornell (1971), pag. 65. The results reported in Fig. 10.8 come from a reanalysis of data collected by the quoted group, assuming a equal contribution from processes $e^+e^- \longrightarrow$ $= \pi^+\pi^-\pi^+\pi^-$ and $\pi^+\pi^-\pi^0\pi^0$. These results have been presented by V.A. Sidorov at the Informal Meeting on Electromagnetic Interactions (Frascati, May 1972).

(33) - G. Barbiellini, M. Conversi, M. Grilli, M. Nigro, L. Paoluzi, P. Spillantini, V. Valente, R. Visentin, and G.T. Zorn: Hadron production by e^+e^- colliding beams in the GeV region, Presented at the Informal Meeting on Storage Rings Physics (Frascati, 1970), Unpublished.

(34) - M. Davier, I. Derado, D.C. Fries, F.F. Liu, R.Z. Mozley, A. C. Odian, J. Park, W.P. Swanson, F. Villa and D. Yount, SLAC preprint (June 30, 1971), Presented at the International Symposium on Electron and Photon Interactions at High Energies, Cornell, 1971.

(35) - G. Smadja, H.H. Bingham, W.B. Fretter, W.J. Podolsky, M.S. Rabin, A.H. Rosenfeld, G.P. Post, J. Ballam, G.B. Chadwick, Y. Eisenberg, E. Kogan, K.C. Moddeit, P. Seyboth, I.O. Skillicorn, H. Spitzer and G. Wolf. Work presented at the Experimental Meson Spectroscopy Conference, April 28-29, Philadelphia, Penn. (1972).

(36) - F.R. Arutyunyan and V.A. Tumanyan, Phys. Letters 4, 177 (1963); R.H. Milburn, Phys. Rev. Letters 10, 75 (1963).

(37) - C.H. Llewellyn Smith and A. Pais, Report number COO-3505-21.

(38) - A. Bramon and M. Greco, Lett. Nuovo Cimento 1, 739 (1971) and Frascati LNF-72/20 (to be published on Nuovo Cimento).

(39) - See also:
(a) J.J. Sakurai and D. Schildkneckt, Physics Letters 40 B, 121 (1972).
(b) A. Bramon, E. Etim and M. Greco, Frascati LNF-72/45 (to be published).
(c) T. Kobayashi, Preprint of Dept. of Physics, Tokyo University of Education, Tokyo (1972).

(40) - E. Pelaquier and F.M. Renard, Nucl. Physics B 39, 547 (1972).

(41) - See, for example:
(a) G. Kramer, J.L. Uretsky and F.T. Walsh, Phys. Rev. 3, 719 (1971).
(b) J. Layssac and F.M. Renard, Lett. Nuovo Cimento 1, 197 (1971)
(c) A.M. Altukov and I.B. Khriplovich, Novosibirsk internal report 36/71.
(d) J. Layssac and F.M. Renard, Montepellier preprint PM/71/2 (1971).
(e) G. Kramer, Electron-Positron Interactions - Lectures delivered at 1972 CERN School - Grado (Italy), (1972).

(42) - E.D. Bloom, D.H. Coward, H. De Staebler, I. Drees, G. Miller, L.W. Mo, R.E. Taylor, M. Breidenbach, J.I. Friedman, G.H. Hartmann, H.W. Kendall, Phys. Rev. Letters 23, 930 (1969); M. Breidenbach, J.I. Friedmann, H.W. Kendall, E.D. Bloom, D.H. Coward, H. De Staebler, J. Drees, J.W. Mo, R.E. Taylor, Phys. Rev. Letters 23, 935 (1969).
See also, the rapporteurs talk at Cornell Conference (1971) by

H.W. Kendall. Proceedings of the International Symposium on Electron and Photon Interactions at High Energies, Cornell, pag. 248

(43) - R. Feynmann, Phys. Rev. Letters 23, 1415 (1969).

(44) - See, for example:
(a) S.D. Drell, Rapporteur's talk to the Amsterdam International Conference on Elementary Particles (Amsterdam, 1971).
(b) R. Gatto, Evolution of Particles Physics (ed. Academic Press New York - London, 1970), pag. 138.
(c) B.L. Ioffe and V.A. Khoze, Yerevan internal report EFI--TF-11 (70).

(45) - On this specific point see, for instance:
(a) C.G. Callen Jr. and D. Gross, Princeton preprint (1972).
(b) G. Altarelli and L. Maiani, Internal Report ISS 72/8 (Istituto Superiore di Sanità - Roma), (1972).
(c) E. Etim and Y. Srivastava, Frascati LNF-72/30 (1972) (Submitted for pubblication to Physics Letters).
(d) J. Bjorken and S. Brodsky, Phys. Rev. D 1, 1416 (1970).
(e) R.W. Griffith, Report Bonn University, PT 2-111 (1972).
We wish to thank Drs. E. Etim and Y. Srivastava for interesting discussions on this subject.

(46) - See, for example,
J. Bjorken, Phys. Rev. 148, 1467 (1966).

(47) - M. Gell-Mann, Schladming Lectures (1972).

(48) - M. Han and Y. Nambu, Phys. Rev. 139, 1006 (1965).

(49) - N. Cabibbo, G. Parisi and M. Testa, Lettere Nuovo Cimento 4, 35 (1970).

(50) - For other details we refer the reader to a seminar delivered by one of us (M.C.) at the Erice International School of Sub-nuclear Physics, published in "Elementary Processes at High Energy" (Academic Press, 1971), p. 547.